Geochimica et Cosmochimica Acta 373 (2024) 17–34

Contents lists available at ScienceDirect

Geochimica et Cosmochimica Acta

journal homepage: www.elsevier.com/locate/gca

Young KREEP-like mare volcanism from Oceanus Procellarum

Zaicong Wang [a,1,*], Keqing Zong [a,1], Yiheng Li [a], Jiawei Li [a], Qi He [a], Zongqi Zou [b], Harry Becker [c], Frédéric Moynier [d], James M.D. Day [e], Wen Zhang [a], Yuqi Qian [a], Long Xiao [a], Zhaochu Hu [a], Zhenbing She [a], Hejiu Hui [f], Xiang Wu [a], Yongsheng Liu [a]

[a] State Key Laboratory of Geological Processes and Mineral Resources, School of Earth Sciences, China University of Geosciences, Wuhan 430074, China
[b] State Key Laboratory of Isotope Geochemistry, Guangzhou Institute of Geochemistry, Chinese Academy of Sciences, Guangzhou 510640, China
[c] Freie Universität Berlin, Institut für Geologische Wissenschaften, Malteserstrasse 74-100, Berlin 12249, Germany
[d] Université de Paris Cité, Institut de Physique du Globe de Paris, CNRS, UMR 7154, 75005 Paris, France
[e] Scripps Institution of Oceanography, University of California San Diego, La Jolla, CA 92093-0244, USA
[f] State Key Laboratory for Mineral Deposits Research & Lunar and Planetary Science Institute, School of Earth Sciences and Engineering, Nanjing University, Nanjing 210023, China

ARTICLE INFO

Associate editor: Janne Blichert-Toft

Keywords:
Chang'e-5
Mare basalt
KREEP
Lunar young volcanism
Oceanus Procellarum

ABSTRACT

The Moon's mare volcanism predominantly occurs within the Procellarum KREEP Terrane (PKT), which is widely thought to be associated with KREEP components within the lunar interior. The Chang'e-5 (CE-5) mission sampled a young (2 Ga) mare basalt Em4/P58 unit of northern Oceanus Procellarum. The geochemistry of the CE-5 mare basalt enables assessment of mantle source compositions which are essential to understand the thermo-chemical mechanism for prolonged volcanism during secular cooling of the Moon. Geochemical compositions of the CE-5 bulk soil, breccias, and basalt clasts from various depths within the drill core consistently display high concentrations of incompatible trace elements (ITE: ~ 0.3 × high-K KREEP; ~ 5 μg/g Th) with KREEP-like inter-element ratios, for example for La/Sm, Nb/Ta, and Zr/Y. Exotic impact ejecta, extensive magma differentiation (<70 % fractional crystallization) and significant assimilation of KREEP materials during magma transit and eruption cannot account for the ITE contents and ratios or radiogenic isotope compositions (e.g., $\varepsilon Nd_{initial}$ of + 8 to + 9 and $\varepsilon Hf_{initial}$ of + 40 to + 46) of the CE-5 basalts; instead, partial melting of their mantle source played a dominant role. The Chang'e-5 basalt is a chemically evolved low-Ti mare basalt (Mg# of ~ 34) with enriched KREEP-like ITE compositions but high long-term time-integrated Sm/Nd and Lu/Hf ratios, which represent a hitherto unsampled type of mare basalt. It formed by melting of an augite-rich mantle source (late-stage magma ocean cumulates containing > 30–60 % augite, and little or no ilmenite), with a small amount of late-stage interstitial melt that resembles KREEP (~1–1.5 modal %, equivalent to 0.2–0.3 μg/g Th in the mantle source). The voluminous mare basalts making up the Em4/P58 unit (>1500 km^3) provide compelling evidence for large-scale, ITE enriched young mare magmatism within Oceanus Procellarum. In combination with remote sensing data and with the unique Th-rich Apollo 12 basalt fragment 12032,366–18 (impact ejecta likely from Oceanus Procellarum), this implies that significant portions of the FeO- and Th-rich mare regions of the western PKT may also have formed in a similar way.

1. Introduction

The Moon's Procellarum KREEP Terrane (PKT, Fig. 1) is characterized by high concentrations of incompatible trace elements (ITE), represented by potassium [K], rare earth element [REE] and phosphorous [P] (hence, KREEP), demarcating a profound lunar compositional surface asymmetry (Haskin et al., 2000; Jolliff et al., 2000; Lawrence et al., 1998). The PKT also hosts extensive mare basalt volcanism over a prolonged period of the Moon's history from at least ~ 4.1 until ~1.2 Ga (Hiesinger et al., 2011; Morota et al., 2011), which is widely thought to be associated with the KREEP enrichment of the PKT (e.g., Jolliff et al., 2000; Laneuville et al., 2013; Wieczorek and Phillips, 2000). Examining

* Corresponding author.
E-mail address: zaicongwang@cug.edu.cn (Z. Wang).
[1] These authors contributed equally to this work.

https://doi.org/10.1016/j.gca.2024.03.029
Received 19 August 2023; Accepted 27 March 2024
Available online 28 March 2024

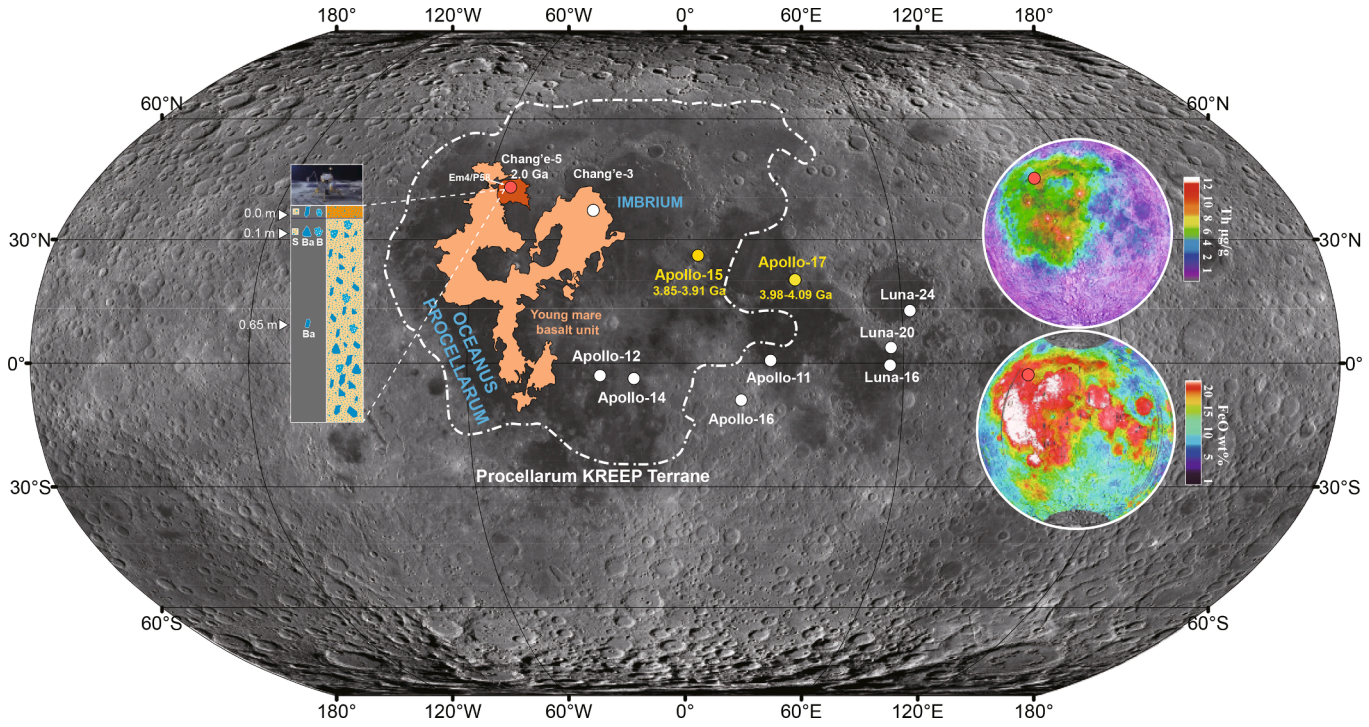

Fig. 1. Spatial distribution of CE-5 basalts in Em4/P58 unit (red) and other young mare basalts (Qian et al., 2023) within the PKT defined by remote sensing data (Jolliff et al., 2000) (outlined by dashed white line). These units show high-Fe, mid-Ti contents and abundant augites, as revealed by the CE-5 and CE-3 missions (Ling et al., 2015; Qian et al., 2023; Zhang et al., 2015). The Apollo 15 and 17 landing sites with indigenous KREEP basalts are shown in yellow circles. CE-5 scooped and drilled soil (S), their basalt (Ba), breccia (B) and agglutinate (A) components were measured in this study. The contour plots of FeO and Th contents of lunar nearside are originally from Jolliff et al. (2000).

the origin and distribution of KREEP-rich igneous rocks is therefore crucial for deciphering the Moon's thermo-chemical evolution (Shearer et al., 2006; Wieczorek et al., 2006).

Samples of KREEP-rich and pristine (i.e., not affected by impacts) basalts, however, are surprisingly rare, including in the KREEP-rich PKT terrane (Shearer et al., 2006; Wieczorek et al., 2006). Most lunar mare basalts (e.g., Borg et al., 2019; Hallis et al., 2014; Neal, 2001) and basaltic meteorites (e.g., Korotev, 2005; Korotev and Irving, 2021) have low Th abundances (< 2 μg/g). Surface enrichment of KREEP components as observed from orbital investigations of Th are often considered to reflect remote impact ejecta or impact mixing with an underlying KREEP-rich substrate (e.g., Haskin, 1998; Wieczorek et al., 2006). Moreover, indigenous KREEP basalts discovered at the Apollo landing sites erupted between ~ 4.1 and 3.8 Ga (Nyquist and Shih, 1992; Shih et al., 1992) and are not representative of younger PKT volcanism. Young mare basalts of Oceanus Procellarum display high abundances of FeO, Th and K (Jolliff et al., 2000; Prettyman et al., 2006), making them underrepresented in comparison to the rock record at the Apollo and Luna landing sites (Prettyman et al., 2006; Qian et al., 2023). A noteworthy case is from the Apollo 12 basalt fragment 12032,366–18 (2.3 Ga?, impact ejecta likely from Oceanus Procellarum) which is unique given its distinct chemical composition with high Th (6.9 μg/g; Stadermann et al., 2022). Due to limited sampling by existing missions (Fig. 1), available lunar basalt samples are unable to well address the origin of young basalts in the PKT region that are enriched in K and Th contents (e.g., Shearer et al., 2006; Wieczorek et al., 2006).

Lunar basalts with KREEP components (i.e., KREEPy basalts) mainly display two trace elemental traits: 1) high ITE concentrations; and 2) ratios of a wide range of ITE close to the theoretical urKREEP composition (often represented by high-K KREEP basalts) (Warren, 1989; Warren and Wasson, 1979). Moreover, the typical pristine KREEP basalts such as Apollo 15,386 and 72,275 have radiogenic Sr and unradiogenic Nd and Hf isotope compositions, as expected from time-integrated LREE-enriched compositions with high Rb/Sr, low Sm/Nd and Lu/Hf ratios in their mantle sources (e.g., Borg and Carlson, 2023; Nyquist and Shih, 1992; Shih et al., 1992; Sprung et al., 2013). Whether the orbital data of enrichment of K and Th in the PKT region reflects the presence of KREEP basalts or merely their high ITE contents (without KREEP-like ITE ratios or enriched radiogenic isotopes) is poorly understood. However, this is important in the interpretation of the remote sensing-based definition of the PKT terrane and requires detailed studies of their indigenous trace element and radiogenic isotope compositions.

The Chinese Chang'e-5 (CE-5) mission sampled the Em4/P58 unit of northern Oceanus Procellarum, which represents large-scale (> 1500 km^3 assuming a thickness of several tens of meters), young (~2.0 Ga) mare volcanism (e.g., Che et al., 2021; Du et al., 2022; Li et al., 2021; Qian et al., 2023; Qian et al., 2021; Tian et al., 2023b; Wang et al., 2023). This type of volcanism has high FeO and Th contents, providing an ideal ground-truth verification of the chemical components of young basalts in the PKT. Because of relatively unradiogenic Sr and radiogenic Nd isotopes, the CE-5 basalts were interpreted to be derived by low-degree melting of a non-KREEP mantle source, followed by extensive fractional crystallization (Tian et al., 2021; Yang et al., 2022), similar to some ~ 3.0 Ga mare basalt-derived lunar meteorites such as the La Paz Icefield 02,205 mare basalt and NWA 4734 pairs (e.g., Borg et al., 2009; Elardo et al., 2014). However, these lunar meteorites show neither high Th contents nor KREEP-like La/Sm ratios (e.g., Borg et al., 2009; Day et al., 2006; Elardo et al., 2014). The CE-5 soils, impact glasses and basalt fragments display high concentrations of the REE with KREEP-like patterns (e.g., Chen et al., 2023; Jiang et al., 2023; Li et al., 2022; Tian et al., 2021; Zong et al., 2022) and KREEP-rich breccia occurs in Chang'e-5 regolith (Mei et al., 2023). However, whether CE-5 basalts show an inherent KREEP signature has not been well established given incomplete data for a wide range of highly incompatible elements. It is also unclear if the KREEP-like component, if present, resulted from either mantle source, magma differentiation or assimilation during

magma ascent. Overall, the likely constituents of the mantle source of the CE-5 basalts remain poorly understood and the affinity of CE-5 basalt to either low-Ti basalt or high-Ti basalt is also debated (e.g., Fu et al., 2022; Jiang et al., 2022; Tian et al., 2023a).

The CE-5 scooped soil has been well studied for chemical composition (Li et al., 2022; Yao et al., 2022; Zong et al., 2022). To add to these works, we measured bulk chemical compositions of drilled soils, breccias, agglutinates, and basalt clasts from various depths of the CE-5 drill cores (Fig. 1). These analyses involved determination of 48 major and trace elements of aliquots of 12 subsamples, and Lu-Hf isotope data for three samples. In-situ analyses on chemical compositions of pyroxene were also carried out to evaluate the effects of crystal fractionation and assimilation on ratios of the ITE. We synthesize the available data and identify CE-5 basalt as a highly evolved mare basalt with a KREEP-like ITE signature but depleted compositions in radiogenic isotopes, which is not represented in the Apollo and Luna catalogs. The comprehensive

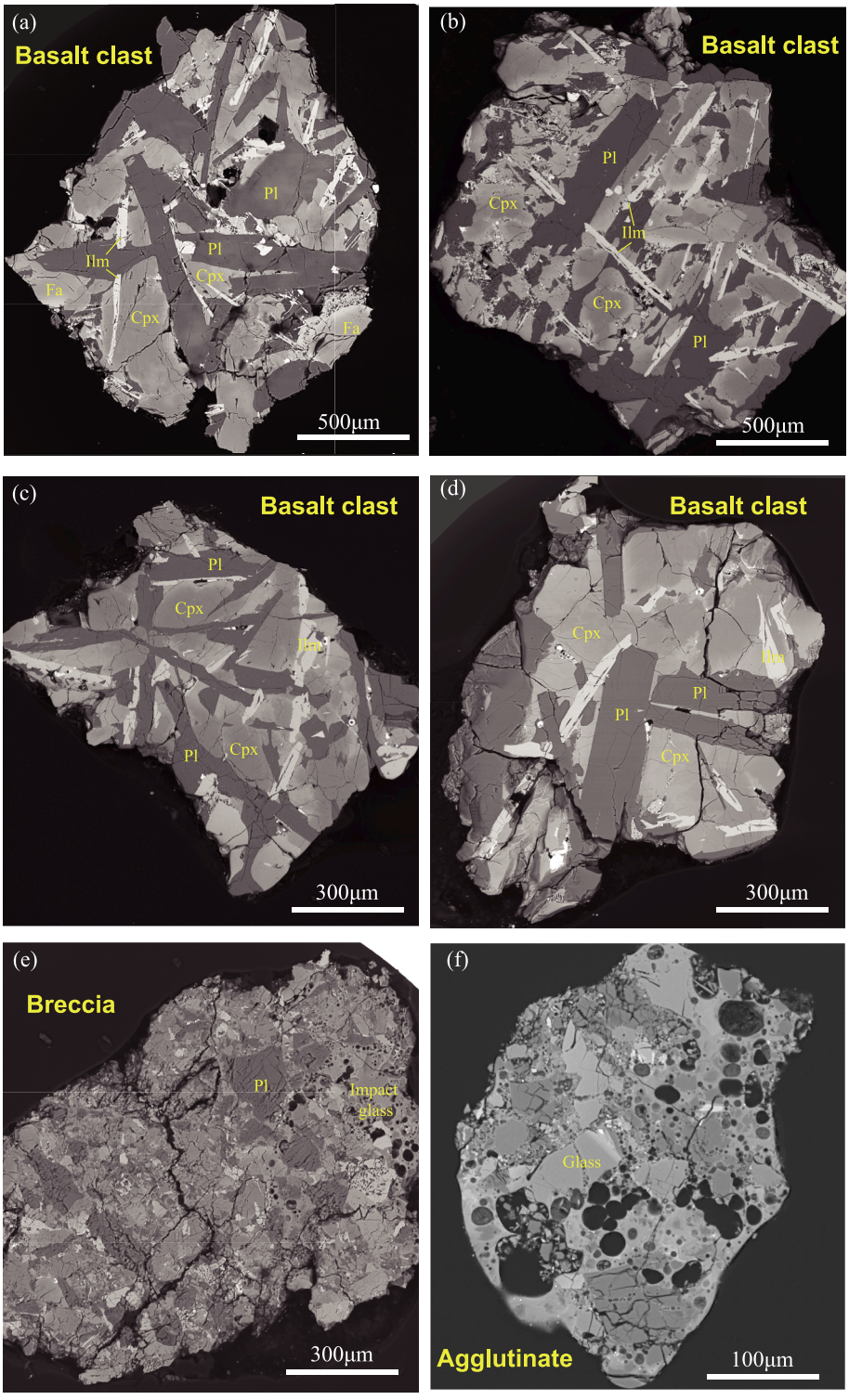

Fig. 2. Representative backscattered electron images of basalt clasts, breccias, and agglutinates. Four basalt clasts (a-d) have subophitic textures and mainly consist of clinopyroxene, plagioclase, ilmenite, and fayalite. Breccia (e) and agglutinate (f) contain several impact glasses and relict mineral crystals.

elemental and isotopic compositions reflect that its mantle source was abundant in augite cumulates expected from the later-stages of lunar magma ocean (LMO) crystallization with a small amount of KREEP-like interstitial melt but absence of ilmenite. The results provide evidence for large-scale, ITE enriched young magmatism within the mare region of the Oceanus Procellarum and even a wider range of the western PKT.

2. Chang'e-5 samples and analytical methods

Three batches (200 mg of CE5C0400, 100 mg of CE5Z0204YJ, and 100 mg of CE5Z0906YJ) of CE-5 lunar soil that were not sieved during sampling and preparation, were obtained from the China National Space Administration Agency. CE5C0400 is a scooped soil while CE5Z0204YJ and CE5Z0906YJ are from soil drill cores. CE5Z0204YJ is from the fourth interval of the second section in the sampling tube (from a depth of ~ 65 cm) and CE5Z0906YJ is from the sixth interval of the ninth section in the sampling tube (~ 10 cm) (Zhao et al., 2023).

In this study, CE-5 lunar soils of variable depth and of different components, particularly basalt clasts, were analyzed for bulk chemistry at the China University of Geosciences, Wuhan (CUGW). Large soil components (i.e., breccias, agglutinates, and basalt fragments, typically 0.5–1.5 mm in size) were manually picked from the lunar soil (Fig. 2). They were cut into two parts with a diamond wire saw. One part was chemically digested for bulk rock measurement of major and trace element abundances and the other portion was utilized for petrographic observations. As shown in Fig. 2, the basalt clasts have a well-preserved igneous texture with no or minor modification by impacts; while breccias and agglutinates mainly consist of impact glass and relict crystals, and highly vesicular nature with small metal-blebs occurs within the agglutinate (Fig. 2f).

The sample digestion and measurement procedures have been well described before and applied to scooped soil, two basalt clasts and other lunar meteorites (Jiang et al., 2023; Zong et al., 2022). This method consumes limited sample but enables simultaneously quantitative analysis of abundances for up to 48 major and trace elements from the same sample aliquot with high precision (Zong et al., 2022). An Agilent 7700x ICP-MS (Agilent Technologies) was used for major and trace element measurements. The detailed operating conditions and acquisition parameters of the ICP-MS, and data reduction procedure have been described before (Zong et al., 2022). International basalt standard reference materials BCR-2 and BHVO-2 were used as monitor standards and their results match well with recommended values (Jiang et al., 2023; Zong et al., 2022).

After ICP-MS analysis, the leftover solutions of scooped soil and basalt clasts were used for Hf isotope analyses. The digested samples were converted to the matrix of 3 M HCl and loaded to an ion exchange column (with Ln-Spec anionic resin) that was leached and balanced by 3 M HCl. Five milliliter 3 M HCl and 6 M HCl were then added twice and 4 times, respectively, which can effectively separate Yb and Lu from Hf. Afterwards, 35 ml 4 M HCl combined with 0.5% H_2O_2 was added to separate Ti. Lastly, 5 ml 2 M HF was used to collect Hf for its isotopic determination using a Neptune Plus MC-ICP-MS (Thermo Fisher Scientific, Bremen, Germany) at CUGW (Lin et al., 2020).

Major and trace element abundances of clinopyroxenes from soils and the basalt clasts were analyzed by laser-ablation ICP-MS, following methods that have been well established at CUGW (Hu et al., 2008). The spot diameter in this study was 32 μm. The measured elements were externally calibrated by using multiple USGS glasses (BCR-2G, BHVO-2G, and BIR-1G). The NIST SRM 610 glass was employed to monitor data quality. The software ICPMSDataCal was used for offline selection and integration of the background and analyzed areas, time-drift correction, and data reduction (Liu et al., 2008). Major and trace element results using laser-ablation ICP-MS are given in Table S3.

3. Results

The major and trace elements of aliquots of 12 subsamples (three drilled soil samples, three breccias, two agglutinates, and four basalt clasts) are reported in the Supplementary Table S1. Different aliquots of CE-5 drill core soil display uniform major and trace element abundances at 2–4 mg sample sizes (within a few percent uncertainty of relative standard deviation, RSD, Figs. S1-S2), and they are also identical with the well-characterized scooped soil (Figs. 3-5). However, abundances of some siderophile elements (e.g., Ni) and volatile elements (e.g., Zn) in the CE-5 soils exhibit scatter (Figs. S1-S2). For agglutinates and breccias, most major and trace elemental compositions of several replicates show a certain range with 20–30% RSD, and the Ni content is also heterogeneous within soil subsamples (Figs. S1-S2). In contrast, basalt clasts show noticeable variations in chemical compositions (e.g., a two-fold range for the ITE concentrations, Fig. 5, Table S1). However, the ratios of the ITE of these basalt clasts (e.g., La/Sm, Zr/Y, Th/U, Eu*) are uniform (Figs. 5-7, Table S1), and the mean values of basalt clasts analyzed (n=6, Table S1) overall are similar to those of the bulk soils (Fig. 3).

The Hf isotopes of two scooped soils and one basalt clast (Table S2) show that the soil subsamples have similar initial $\varepsilon Hf_{(2.0\ Ga)}$ of + 40 to +42 and are lower than that of the basalt clast (+46, Fig. 8a). Clinopyroxene grains measured for compositions shows variable Mg# from 60 to <10, which resulted from strong magmatic fractionation (Table S3, Fig. 9). Although incompatible elements like the REE of these clinopyroxene show large variations in concentration, although the La/Sm ratios and Eu* are quite constant (Fig. 9).

4. Discussion

4.1. Chemical compositions of CE-5 soil and its components

The scooped soil of CE-5 has been well-characterized from different batches (CE5C0400, CE5C0600, CE5C0800) and using different methods (ICP-MS and INAA, XRF); they show rather homogenous chemical compositions (Li et al., 2022; Yao et al., 2022; Zong et al., 2022). In this study, we further analyzed milligram-sized samples of drilled soils of variable depths and their different components (Table S1, Figs. S1-S2). Subsamples of the drilled soil demonstrate consistent chemical compositions and match those of the scooped soil within analytical uncertainty (Fig. 3). These results indicate that the CE-5 soil, at least from shallow depths, is homogenous in chemical composition at the milligram level, except for a few elements such as Ni and Zn which are likely to have been affected by variable degrees of meteoroid addition or condensation/evaporation occurring as a result of impacts that formed the soil (e.g., Yang et al., 2022; Zong et al., 2022). Such homogeneity can be ascribed to the very small particle sizes of the CE-5 soil (> 95% of particles are less than 10 μm) (e.g., Cao et al., 2022; Li et al., 2022; Zong et al., 2022). Apart from Ni, major and trace elemental compositions of agglutinates and breccias overlap the scooped soil within 20–30% RSD (Fig. S1-S2). The elevated Ni contents for bulk soil, agglutinates and breccias are consistent with their petrological features (Fig. 2), reflecting the variable effects of meteoroid impacts, which are known to elevate Ni contents considerably (e.g., Day, 2020).

Different basalt clasts show variable major elements abundances, as reflected by this study (Fig. 4) and previous works (e.g., Che et al., 2021; Chen et al., 2023; Su et al., 2022). These examined basalt clasts are often 0.5–1.5 mm size, equivalent to several milligrams (e.g., Fig. 2 and Table S1). Most trace elements (e.g., Cr, Y, Zr, REE, Hf, Th, and U) of these basalt clasts show variations in concentration by a factor of two (Fig. 5 and S2). Such chemical variations could be ascribed to the 'mode effect' at small sample sizes (i.e., different proportions of mineral phases and mesostasis in different basalt clasts). The FeO concentration of basalt clasts is slightly elevated relative to bulk soils (e.g., 25.3 wt% versus 22.7 wt%). We also note that the Mg# (molar ratio of Mg/

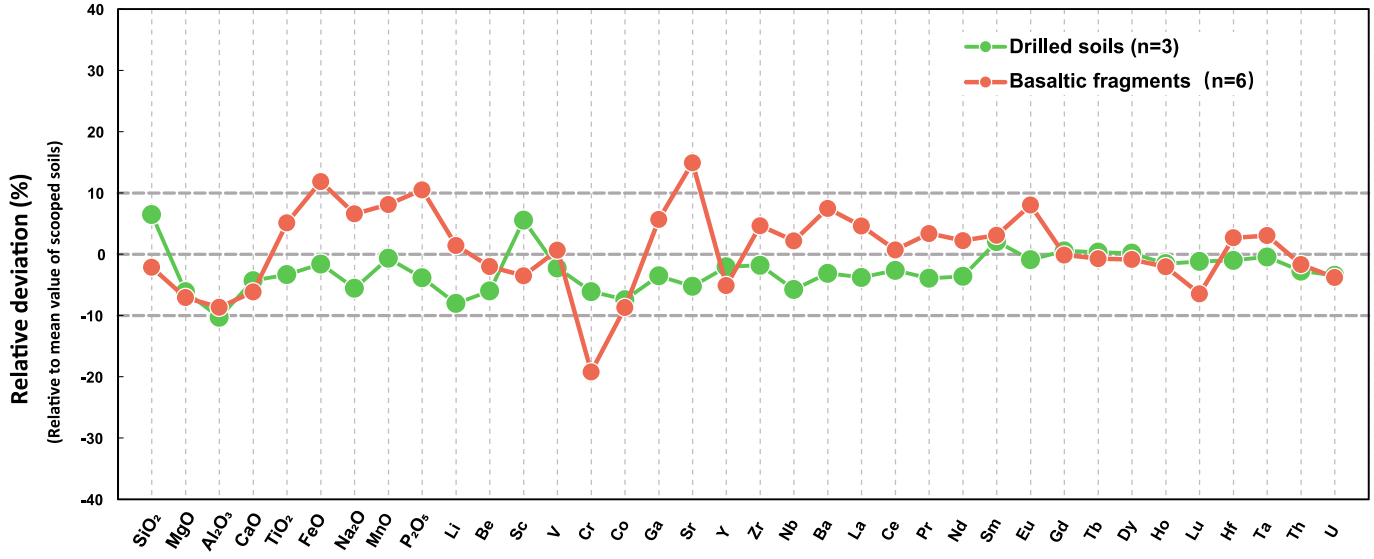

Fig. 3. The relative deviation (RE%) of the average compositions of drilled soil and basalt clasts compared to the mean value of scooped soil (Zong et al., 2022).

(Mg+Fe)) of most basalt clasts are lower than bulk soil (e.g., 28 versus 34) (Table S1 and Chen et al., 2023). These features likely reflect that the basalt clasts tend to sample more evolved parts of CE-5 basalt, and higher proportions of Fe-rich phases. However, the ratios of ITE of these basalt clasts (e.g., La/Sm, Zr/Y, Th/U) are uniform (Fig. 5 and 7, Table S1). Heterogenous sampling or magmatic fractionation can lead to noticeable changes in concentrations but have limited effects on ratios of ITE, which has been also well illustrated for the Apollo 17 KREEPy basalt (Salpas et al., 1987).

The scooped and drilled soils demonstrate consistent compositions, implying either limited addition of exotic materials into the CE-5 soil or addition of similar materials. As shown in Fig. 2, the basalt clasts display no evidence of post-crystallization modifications and low Ni contents (about 20 μg/g, Table S1), they are therefore likely to represent relatively pristine CE-5 basaltic materials. Importantly, the ratios of Zr/Y, La/Sm, and Nb/Ta in basalt clasts overlap those of bulk soils and impact glasses (Fig. 5). The CE-5 soil underwent long-term impact and strong modification (e.g., Li et al., 2023; Long et al., 2022; Yang et al., 2022); and a small fraction of exotic ejecta from units outside of the CE5 basalt has been identified (e.g., Jia et al., 2022; Mei et al., 2023; Zeng et al., 2022; Zhao et al., 2023). However, such effect was overall limited for the bulk composition of the CE-5 soil as demonstrated here. The remarkable homogeneity of the CE-5 lunar soil, and the consistency of ITE ratios of bulk soil and basalt clasts, leads us to conclude that the CE-5 soil formed mainly (likely > 95%) from the local basalts of the Em5/P58 unit, consistent with increasing evidence from other studies (e.g., Jia et al., 2021; Yang et al., 2022; Zeng et al., 2022; Zong et al., 2022). Because the bulk soil is likely representative of a large homogeneous component of CE-5 basalts, its bulk chemical composition likely overall reflects the mean value of the sampled CE-5 basalt, except for some volatile and/or siderophile elements.

4.2. Low-Ti affinity of Chang'e-5 mare basalts

The CE-5 basalts are from the Em4/P58 unit of mare basalts within the northern Oceanus Procellarum. Which type of mare basalt (i.e., very low-Ti, low-Ti, and high-Ti) the CE-5 basalt can be classified as is of great importance to understand their origin and evolution (Neal and Taylor, 1992; Papike et al., 1976). Based on the petrological data and chemical compositions, CE-5 basalts display highly evolved features with low Mg# (34), high FeO (22.5 wt%), intermediate TiO_2 (5.1 wt%) and low Ni contents (20 μg/g, Table S1) (e.g., Chen et al., 2023; He et al., 2022; Li et al., 2022; Yang et al., 2023). The abundant ilmenite (2–6 vol %) in basalt clasts (e.g., Cao et al., 2022; Chen et al., 2023; Li et al., 2022) and the TiO_2 contents of CE-5 basalt may have resulted from extensive fractionation (e.g., He et al., 2022; Tian et al., 2021; Yang et al., 2023). Its primarily melt likely contains 4.4 wt% or lower TiO_2 (Zhang et al., 2022), which lies within the range of low-Ti mare basalts (Neal and Taylor, 1992). On the other hand, the Fe# (Fe/(Fe+Mg) molar ratio) -Ti# (Ti/(Ti+Cr) molar ratio) relationship of pyroxenes represents another powerful indicator of basalt type (e.g., Arai et al., 1996; Robinson et al., 2012). This method indicates an affinity of CE-5 basalt to the high-Ti mare basalt type (Fu et al., 2022), which apparently also explains the presence of some high-Ti CE-5 fragments (Jiang et al., 2022). Because Cr is highly compatible relative to Ti in clinopyroxene (e.g., Dygert et al., 2014; Leitzke et al., 2016), progressive magmatic differentiation may account for the elevated Ti# of clinopyroxene with higher Fe# (Tian et al., 2023a). However, such a process is unlikely to be the main cause of the elevated Ti#, because it is appliable to all mare basalts and, importantly, the Ti# of early crystallized clinopyroxene (e.g., at given Fe# of 40–50) remains higher for CE-5 basalt than for characteristic low-Ti Apollo mare basalts (Fig. 8b). Such an apparent discrepancy reflects a high proportion of augite in the mantle source of CE-5 basalts, as discussed below.

The correlation of Nd-Hf isotope ratios of mare basalts is well-suited to distinguish between a low- and a high-Ti mare basalt nomenclature for the CE-5 basalt. Ilmenite tends to incorporate much more Hf than the REE and is a predominant mineral responsible for noticeable differentiation of Lu/Hf ratio without perturbing the Sm/Nd system. Lunar low-Ti and high-Ti basalts therefore display distinct trends for Nd-Hf isotopes (e.g., Beard et al., 1998; Münker, 2010; Sprung et al., 2013; Unruh et al., 1984). All low-Ti mare basalts, including Apollo 12 ilmenite mare basalts, share consistent Lu/Hf-Sm/Nd ratios, although they display significant Nd-Hf isotope variability (Fig. 8a). The $\varepsilon Nd_{initial}$ of CE-5 basalt (~ +8 to +9) has been obtained from in-situ analyses on merrillite (Tian et al., 2021). We show that the CE-5 soil and basalt clasts have similar $\varepsilon Hf_{initial}$ of +40 to +46, leading to its Hf-Nd isotope compositions being consistent with the trends of low-Ti basalt and distinct from the high-Ti basalt trend (Fig. 8a). The exposure of samples on the lunar surface to cosmic rays often leads to isotope anomalies in many elements, and correcting neutron capture effects has been shown to be important for Hf isotopes of some lunar rocks (e.g., Gaffney and Borg, 2014; Sprung et al., 2013). We did not obtain other isotopes of Hf due to limits of the available quantity of sample so that such correction is impossible in this study. However, neutron capture effects do not necessarily occur for all lunar samples, e.g., for many low-Ti basalts (See Fig. 8a and Sprung et al., 2013), and the

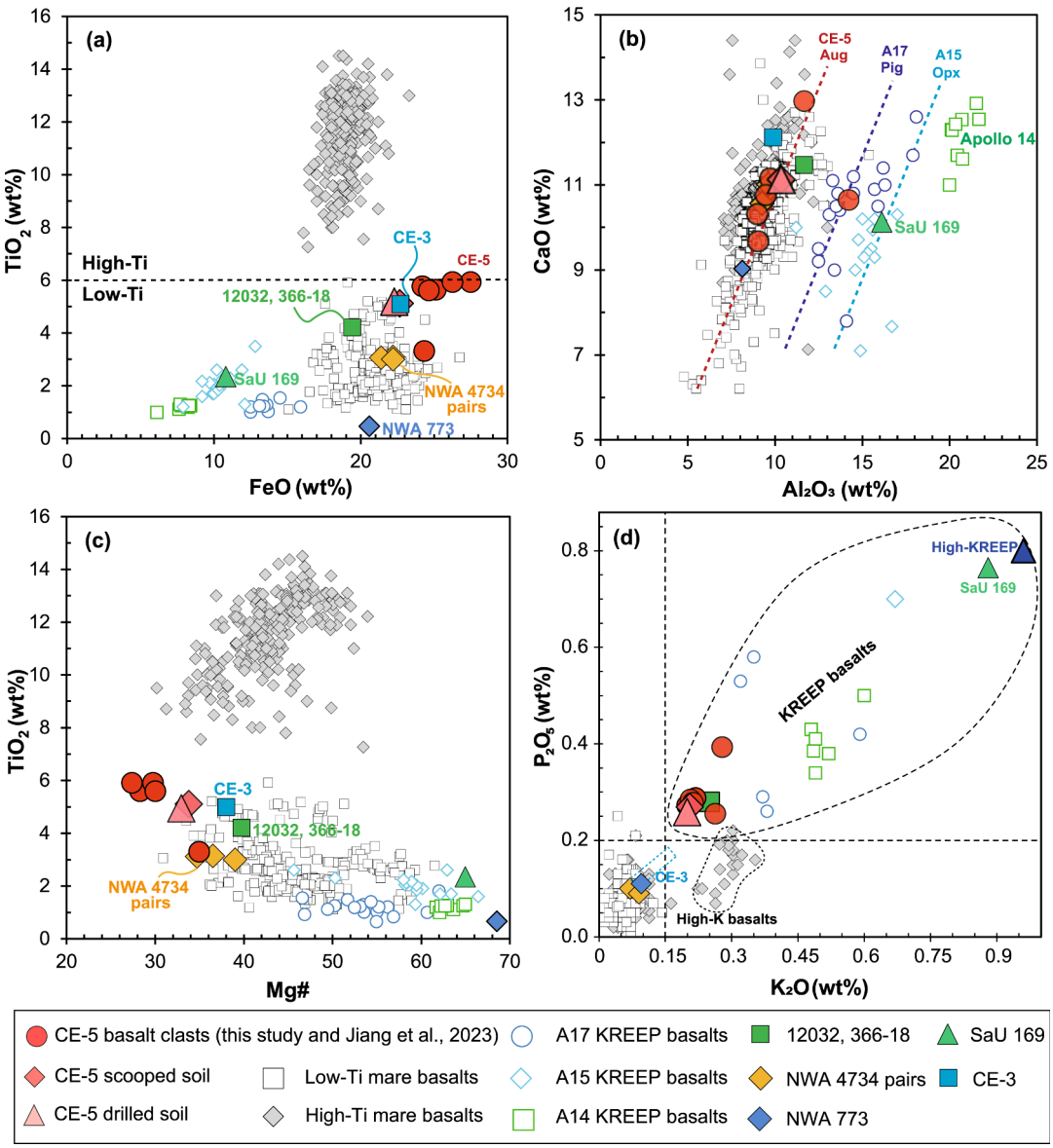

Fig. 4. Major elements of CE-5 soil and its components. Basalts from CE-5 and CE-3 landing sites (Ling et al., 2015; Zhang et al., 2015) and the KREEP-bearing basalt fragment Apollo 12032,366–18 (Stadermann et al., 2022) show similar major elements, overlapping with evolved low-Ti mare basalts with similarly low Mg# value, including NWA 4734, NWA 032 and LAP 02205 pairs (yellow diamonds) (Borg et al., 2009; Elardo et al., 2014). However, CE-5 and Apollo 12032,366–18 display higher K_2O and P_2O_5 contents than low-Ti mare basalts (d). Note that CE-5 basalt (augite-rich) shows lower Mg# but higher CaO/Al_2O_3 than Apollo 17 (pigeonite-rich) and 15 (orthopyroxene-rich) KREEP basalts (b), likely reflecting the variable mineralogical control in the mantle sources. The data of low-Ti and high Ti mare basalts are from the Lunar Sample Compendium (https://www-curator.jsc.nasa.gov/lunar/lsc/index.cfm), and others are summarized in Supplementary Table S4.

effect would be lower for the less exposed basalt clasts relative to the soils. The CE-5 soil show $\varepsilon Hf_{initial}$ similar to the basalt clast (Fig. 8a), likely reflecting a limited neutron capture effect on CE-5 basalt, although future more precise work is required for clarification. Based on the currently available Hf-Nd isotopes, we suggest the affinity of CE-5 basalt to low-Ti basalt. The result also reveals negligible ilmenite in the mantle source; otherwise, the abundant ilmenite, if present in the source, would lead to source ratios of Lu/Hf-Sm/Nd close to high-Ti basalts, which is clearly not the case (Fig. 8a). This result is also consistent with the constraints based on pMELTs simulations (Luo et al., 2023).

4.3. KREEP-like ITE compositions in Chang'e-5 mare basalts

4.3.1. KREEP-like signature in CE-5 mare basalts

Although the CE-5 basalt is a low-Ti mare basalt variant, its trace elements differ from known low-Ti mare basalts. For example, the CE-5 basalt has a high Th content (5.1 μg/g) relative to low-Ti mare basalts (Fig. 7 and S3). Overall, the CE-5 bulk soil, basalt clasts and breccia display elevated ITE abundances (e.g., Ba, Th, U, Nb, Ta, Zr, Hf, and REE, ~0.3 × urKREEP or high-K KREEP (Warren, 1989)). Such levels are comparable to the Apollo 72,275 KREEPy basalt clasts with a mean of 5.6 μg/g Th (e.g., Fig. 6,7 and S3). Following the criteria of Warren (1989), high contents of the ITE and KREEP-like ITE ratios should both be satisfied to reflect a KREEP-like trace element composition. For example, high-K basalts typically have high contents of K (>2000 μg/g), Th (2–5 μg/g) and other incompatible elements, a level similar to CE-5 basalt and Apollo 17 KREEP basalts (Fig. 7d and S4). However, high-K basalts are not recognized as KREEPy basalts, because their La/Yb and La/Sm ratios are rather low (Neal and Taylor, 1992). Instead, the KREEP-like samples have high La/Sm (> 2) and La/Yb ratios (typically > 2.9, Fig. 7c and S4).

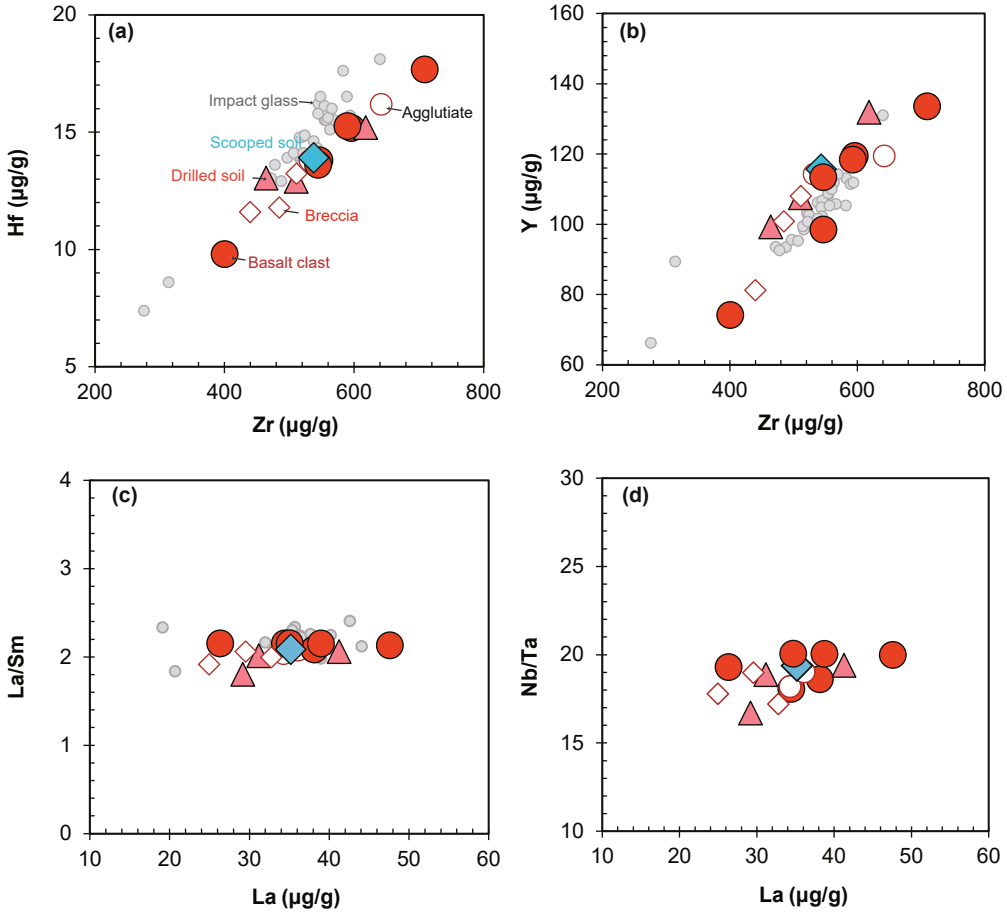

Fig. 5. Concentration and ratios of incompatible trace elements in different components of CE-5 soil. They show variable contents but consistent ratios. Light gray circles are impact glasses (Yang et al., 2022).

The bulk soil, breccia, basalt clasts of CE-5 all display distinct KREEP-like patterns and ratios for incompatible trace elements (e.g., La/Sm, Zr/Y and Nb/Ta, Figs. 6 and 7), which cannot be ascribed to magmatic differentiation. For example, Nb and Ta are highly incompatible in most crystallization phases of lunar basalts except ilmenite, and Nb/Ta is predominantly affected by ilmenite removal or addition during lunar magmatism (e.g., Leitzke et al., 2016; Münker, 2010). Given ilmenite undersaturation during differentiation of the CE-5 parental magma (Zhang et al., 2022), the Nb/Ta ratio of CE-5 basalt reflects parental magma and mantle source. The Na/Ta ratio of CE-5 is similar to those of high-K KREEP and of the 15,386 KREEP basalt, but noticeably higher than for Apollo low-Ti and high-Ti mare basalts (Fig. 7c). Such a high Nb/Ta ratio for KREEP basalts was likely the result of separation of dense Ti-rich cumulates from urKREEP during magma ocean overturn. The Zr/Hf ratio is another indicator of ilmenite involvement (Münker, 2010) and the broad correlation between Zr/Hf and Nb/Ta further supports the separation of Ti-rich cumulates (Fig. 7c). As with Hf isotopes, the Zr/Hf and Nb/Ta ratios of the CE-5 basalt indicate negligible ilmenite in its mantle source. If residual ilmenite was present after partial melting to explain high Nb/Ta ratio, it would be difficult to reconcile with high Nb and Ta contents and Ta/La and Nb/Ce ratios of CE-5 basalts which trend towards urKREEP endmembers (Fig. 6) (e.g., Hui et al., 2013).

Like the aforementioned Apollo KREEP basalts, the CE-5 basalt also shows strong fractionation of the REE, e.g., high ratios of La/Sm (~ 2.1) and La/Yb (~ 3.6, Figs. 6 and 7). These features differ from what is observed for most Apollo mare basalts and this difference is also reflected in other ratios, such as Zr/Y (Fig. 7a). Given the highly evolved nature of CE-5 basalt (e.g., Che et al., 2021; He et al., 2022; Su et al., 2022; Yang et al., 2023), low-degree partial melting and extensive crystallization were proposed to explain such KREEP-like ratios (Tian et al., 2021). However, such process is most likely not the predominant mechanism (Warren and Wasson, 1979). Extensive crystallization can significantly elevate the contents of ITE in melts but hardly change the ratios used to identify the KREEP-like signature, such as La/Sm, Nb/Ta and Zr/Y. As shown in Fig. S6, La/Sm ratio varies less than 20% even if high-degree (< 70%) fractional crystallization occurs. The highly evolved low-Ti mare basalts such as NWA 4734, NWA 032 and LAP 02205 pairs (Borg et al., 2009; Day et al., 2006; Elardo et al., 2014) show low Mg# of 35–40 similar to the CE-5 basalt (Mg# of 34), but their La/Sm and La/Yb ratios are far lower than those of the CE-5 basalt (Fig. 4 and 7).

Our in-situ data on clinopyroxene provide convincing support for this argument. The clinopyroxenes of CE-5 basalt in this study and previous work show variable Mg# covering the least evolved to highly evolved range (from ~ 60 to ⟨10) and a large variation of REE contents (Table S3 and Fig. 9). However, La/Sm ratios and Eu* of these clinopyroxenes with different Mg# are overall constant (Fig. 9), reflecting the negligible effects of extensive fractionation on these ratios. Therefore, the La/Sm ratio and other KREEP-like ratios of CE-5 basalt cannot result from magmatic fractionation but instead reflect the primary signature.

Anomalies of Eu* and Ti/Sm ratio are also often used as indicators for KREEPy basalts (e.g., Borg et al., 2009; McKay et al., 1978), because the urKREEP reservoir is expected to display extremely negative Eu* (0.2) and low Ti/Sm (~500) after extensive (> 95%) crystallization of magma ocean (Warren and Wasson, 1979). However, Eu* and Ti/Sm ratio could not be effective markers. This is because REE and Ti contents in basalts reflect the combined results of KREEP and other cumulate

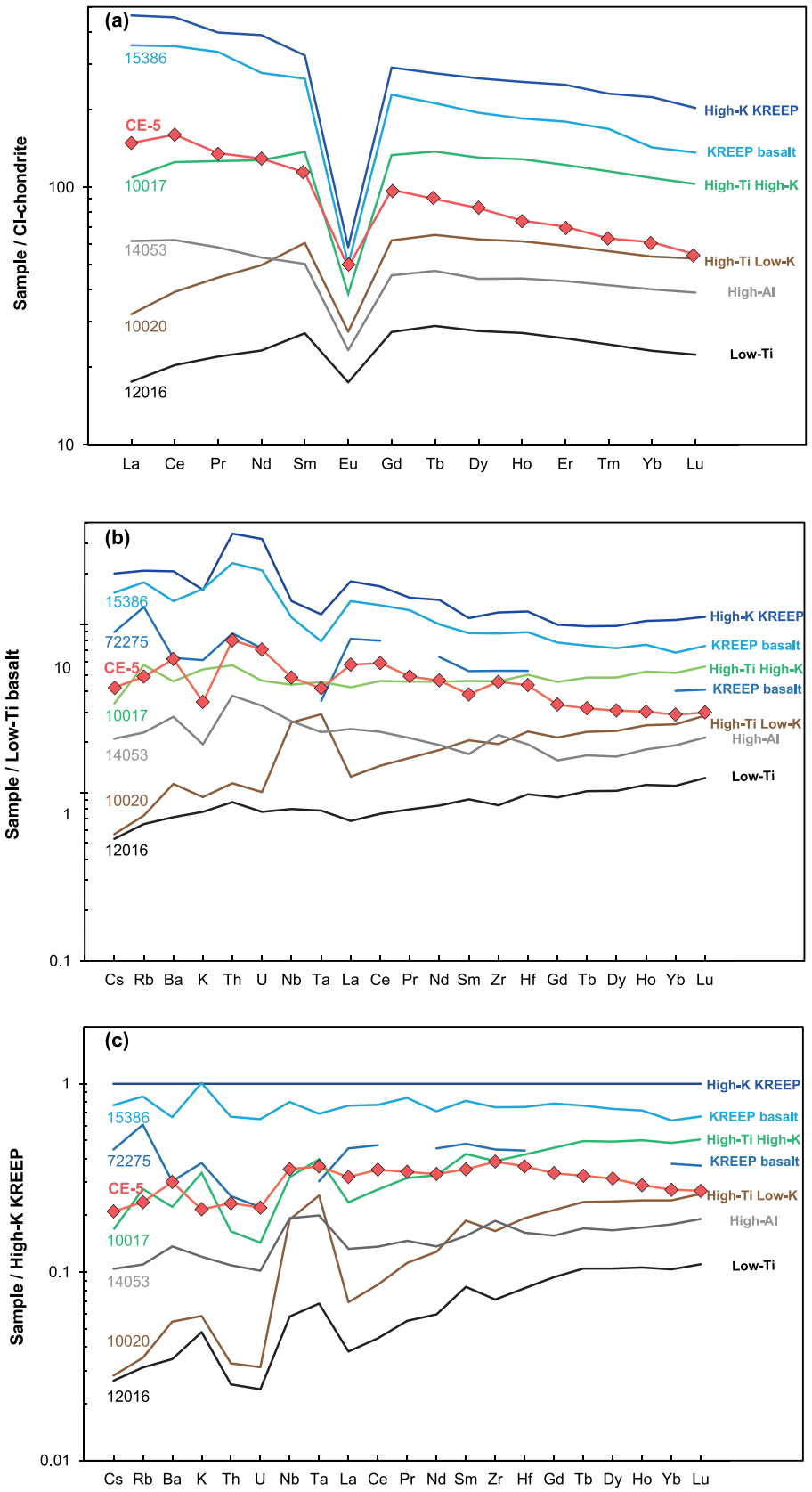

Fig. 6. Trace element compositions of CE-5 basalt. The CE-5 basalt as represented by bulk soil display high ITE contents (about 0.3 × high-K KREEP). The trace elements are normalized to low-Ti basalt or high-K KREEP in order to better display their differences. Data of 10017, 14053, 10,020 and 12,016 are from Hallis et al. (2014), and 15,386 are from Neal and Kramer (2006).

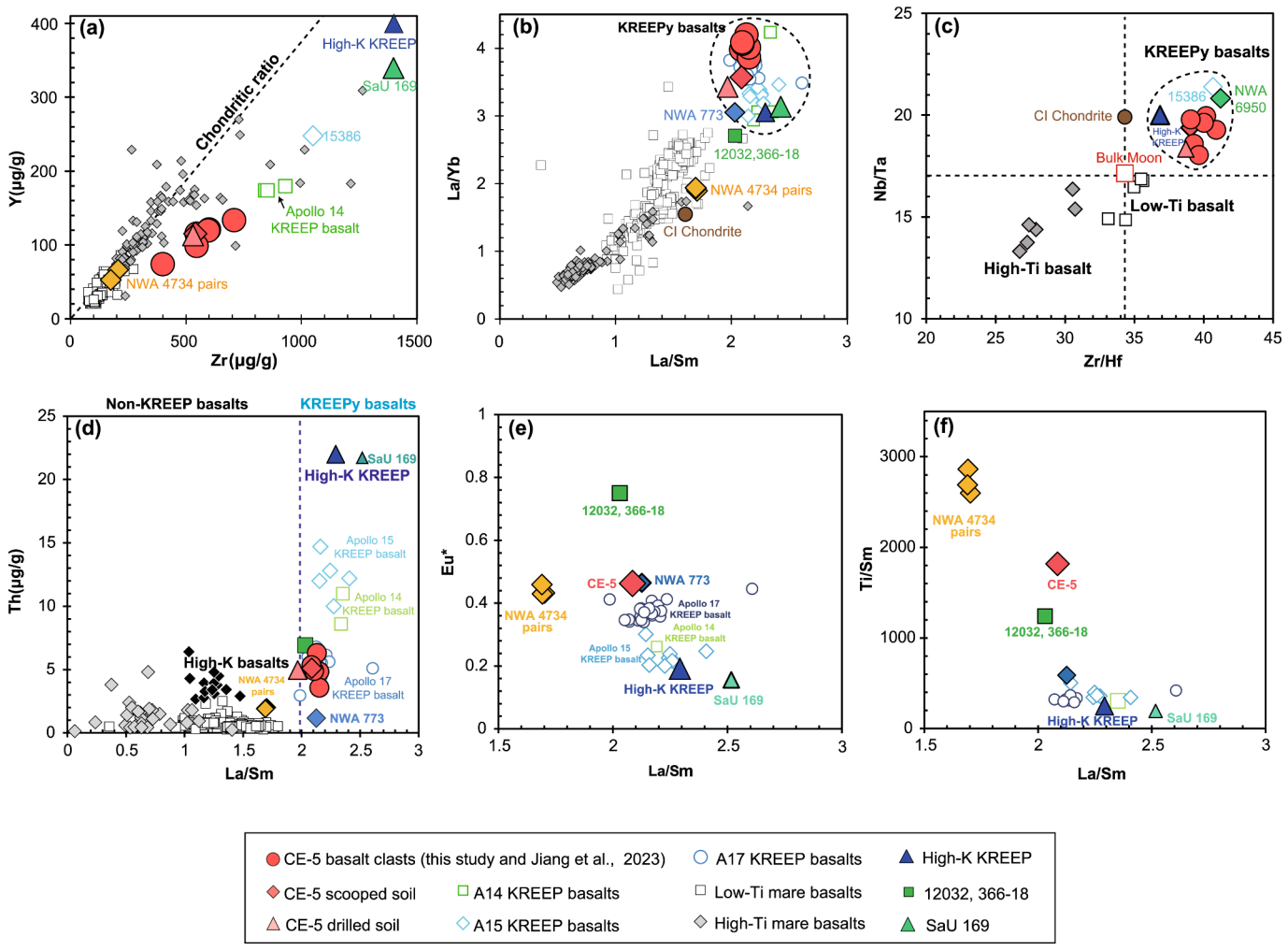

Fig. 7. The KREEP-like ratios of incompatible trace elements of CE-5 basalt. The CE-5 soil and its components show variable ITE contents but constant ratios as other KREEP basalts (e.g., Zr and Y shown, a). Extensive magmatic differentiation (as indicated by NWA4734 pairs [yellow diamonds]) cannot explain high ratios of La/Yb and La/Sm of the CE-5 basalts, which overall overlap KREEP basalts and differ from Apollo low-Ti and high-Ti mare basalts (b, d). Zr/Hf and Nb/Ta (only high-precision Nb-Ta data shown (Münker, 2010)) are also excellent indicators for KREEP signatures (c). NWA 6950 shows KREEP-like signature as NWA 773 clan (Korotev and Irving, 2021) and its Nb/Ta-Zr/Hf ratios obtained by same methods as this study (Zong et al., 2022) are shown for comparison. Lunar KREEPy basalts typically show high La/Sm of > 2 relative to low-Ti and high-Ti mare basalts. CE-5 basalts show high La/Sm and high Th contents but its Eu* and Ti/Sm ratios differ from KREEPy basalts (d-f). Data source as Fig. 4 and see more in Table S4.

phases in the mantle source, particularly clinopyroxene or plagioclase. Consequently, Eu* and Ti/Sm are expected to vary among KREEPy basalts (Fig. 7e-f). The Eu* of CE-5 basalt (0.47, Table S1) is slightly higher than KREEPy samples (Apollo 15&17, SaU 169, and high-K KREEP), but similar to NWA 773 and NWA 4737 pairs (Fig. 7e). The high Ti/Sm ratio of CE-5 basalt can be ascribed to abundant augite in its mantle source (see discussion below).

4.3.2. *Mantle source origin of KREEP-like ITE signature for Chang'e-5 basalt*

A key question is whether the KREEP-like ITE component of CE-5 basalt was inherent to the mantle source or due to contamination during magma ascent. Due to high Rb/Sr, low Sm/Nd and Lu/Hf, urKREEP components that evolved from ~ 4.4 to 2.0 Ga, would show relatively radiogenic Sr and unradiogenic Nd-Hf isotopes (e.g., εNd of −12, Fig. 10c). If assimilation resulted in the KREEP-like ITE properties of CE-5 basalts, such Sr-Nd-Hf isotope signatures would be inherited by CE-5 basalts. However, the young eruption age of the CE-5 basalts and its Sr-Nd-Hf isotopes (e.g., $\varepsilon Nd_{initial}$ of ~ +8 to +9 and $\varepsilon Hf_{initial}$ of ~ +40 to +46) exclude significant late KREEP assimilation (Fig. 10). More critically, it is impossible to simultaneously satisfy the εNd-εHf values and the high La/Yb (~ 3.6) and La/Sm (~ 2.1) ratios that are similar to, or even higher than high-K KREEP and the Apollo 17 KREEP basalts (Fig. 10).

A simple binary mixing model is shown to simulate the trace element abundances and ratios, and Nd isotopes of CE-5 basalts (Fig. 10). Either the primary partial melt derived from a clinopyroxene-rich cumulate source (assimilation in deep mantle depth; Fig. 10a-c) or its evolved melt after 50% fractional crystallization (assimilation in shallow mantle or crust depth; Fig. 10d-f) is assumed to assimilate high-K KREEP. The binary mixing modelling shows that ITE enrichment in CE-5 basalts requires > 25% of KREEP assimilation to account for their trace elements contents (Fig. 10a). The trace element ratios (e.g., La/Sm, Sm/Nd and Nb/Ta) further confirm that > 25% of KREEP assimilation is required (Fig. 10b). Such significant assimilation of KREEP materials (> 25%) would lead to radiogenic Nd isotopes in CE-5 basalts (εNd of < −5, Fig. 10c). However, only < 5–10% of KREEP is required to explain the limited radiogenic ingrowth of Nd isotopes in CE-5 basalts (ε_{Nd} of +8 to +9) (Tian et al., 2021), even if we mixed the partial melts of the most depleted mantle sources with KREEP (Fig. 10). On the other hand, the assimilation of 5–10% KREEP to reconcile the Nd isotopes cannot simultaneously reconcile with around 30% KREEP components and

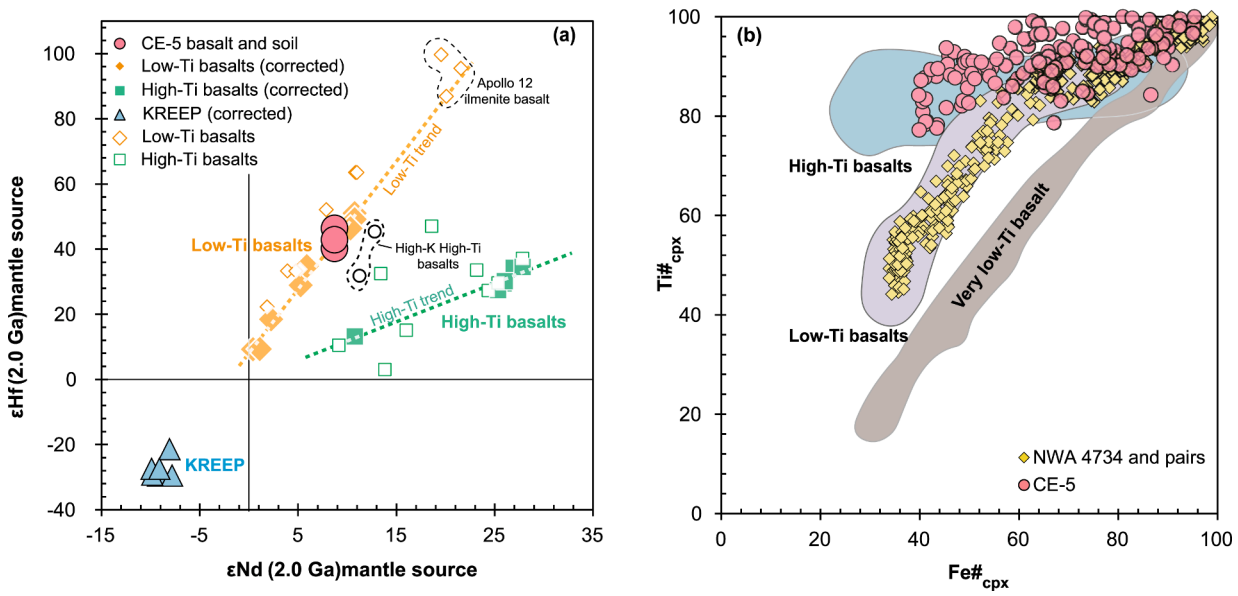

Fig. 8. Neodymium and hafnium isotopes of mantle source and clinopyroxene compositions of CE-5 basalt. (a) The εHf_{source} and εNd_{source} at 2.0 Ga for CE-5 and other lunar basalts were calculated assuming source formation at the time of magma ocean crystallization at 4.35 Ga from a chondritic magma ocean (Borg and Carlson, 2023). The data corrected (filled symbols) for neutron effects on Hf isotopes (Sprung et al., 2013) and uncorrected ones (unfilled symbols) are shown for comparison (Beard et al., 1998; Unruh et al., 1984). The CE-5 lies on the Nd-Hf isotope trend for low-Ti basalts rather than high-Ti basalts. (b) Fields represent Fe# (Fe/(Fe + Mg) molar ratio) versus Ti# (Ti/(Ti + Cr) molar ratio) of clinopyroxene in very low-Ti, low-Ti, and high-Ti mare basalts (Fu et al., 2022; Robinson et al., 2012). The CE-5 data compiled (Fu et al., 2022; Luo et al., 2023; Su et al., 2022) show high Ti# at given Fe#. The highly evolved, low-Ti meteorites NWA 4734 and pairs are shown for comparison (Elardo et al., 2014).

KREEP-like trace element ratios of CE-5 basalts. This conclusion is also applicable to the mixing of evolving melts with KREEP components (Fig. 10d-f). Because most of the trace elements used here are incompatible in olivine and clinopyroxene (Dygert et al., 2020), fractional crystallization would elevate the contents of incompatible elements in the evolving melts but hardly affect their ratios (e.g., La/Sm and Nb/Ta).

For similar reasons, incorporation of considerable KREEP-rich subsurface regolith into lava flows feeding CE-5 basalts must also have been negligible. This conclusion is also supported by in-situ data on crystallizing pyroxene (Fig. 9) and plagioclase (Tian et al., 2022). Therefore, we suggest that assimilation of any KREEP component during magma ascent was not sufficient to affect the CE-5 basalt's KREEP-like ITE composition. Instead, we favor that the KREEP-like ITE signature of the CE-5 basalt was inherited from its mantle source.

Subcrustal KREEP layers have been widely thought to be present at the base of crust and up to several several-km thickness, which is important for lunar thermal evolution (e.g., Hess and Parmentier, 2001; Laneuville et al., 2013; Wieczorek and Phillips, 2000). The voluminous (> 1500 km^3 at the surface, presumably more at depth) magmas of CE-5 basalt (Qian et al., 2021; Tian et al., 2023b; Wang et al., 2023) ascended through the plumbing system and accumulated at the base of lithospheric mantle and crust for extensive fractionation (Luo et al., 2023). However, such melts do not show any noticeable assimilation of KREEP components, suggesting a lack of subcrustal KREEP layer, at least in the Em4/P58 unit.

4.3.3. *Chang'e-5 basalt as a previously unrecognized type of lunar basalt*

Combined with igneous textures and low Ni contents (< 30 μg/g, i.e., no meteoroid addition), it is clear that the CE-5 basalt displays inherently high abundances of ITE with KREEP-like ratios; whereas it also shows depleted radiogenic Sr-Nd-Hf isotopes which differ from the typical KREEP basalts (Fig. 7 and 8). We suggest that the CE-5 basalt is a hitherto unrecognized form of mare basalt with KREEP-like ITE component, which however, is distinct from either the previously described KREEP basalt clasts from the Apollo 15 and 17 landing sites, or known low-Ti mare basalts.

In terms of major elements, the CE-5 basalts show low Mg# (~34) relative to Apollo 15 and 17 KREEP basalts (Mg# of 50–70, Fig. 4 and S5), and were evolved from low-Ti parental melts via fractional crystallization. Apollo 15 (orthopyroxene-rich) and 17 (pigeonite-rich) KREEP basalts (Fig. 4b) are distinguished from mare basalts by their high-Al contents and low Ca/Al ratios (e.g., Ryder, 1987; Ryder et al., 1977; Salpas et al., 1987; Taylor et al., 2012). In contrast, CE-5 basalts contain abundant augite (e.g., Chen et al., 2023; Li et al., 2022; Qian et al., 2023) and have high FeO contents and high Ca/Al (Fig. 4b), reflecting enrichment of Ca-rich clinopyroxene in their mantle source. The young basalts show similar major element compositions (e.g., low Mg# and high Fe contents) to the KREEP-poor YAMM basalts (Srivastava et al., 2022) and NWA 4734 and 032 pairs (Borg et al., 2009; Elardo et al., 2014), and are low-Ti mare basalts.

From a trace element perspective, the CE-5 basalt displays ITE abundances and ratios comparable to KREEPy basalt such as 72,275 but noticeably different from Apollo and meteorite low-Ti mare basalts (Figs. 6 and 7). However, isotopically, the CE-5 basalt is not enriched in radiogenic Sr-Nd-Hf isotopes as the KREEP basalts. Therefore, the CE-5 basalt likely represents a new type of low-Ti mare basalts that show mineralogical and major element characteristics similar to highly evolved low-Ti mare basalts but ITE compositions similar to KREEP basalts. The CE-5 basalts have been underrepresented in the available lunar sample collections and broaden the sampled diversity of lunar mare basalts.

4.4. *KREEP-bearing and augite-rich cumulate source*

The CE-5 basalts show a KREEP-like signature for most highly incompatible elements. However, its Sr-Nd-Hf isotope compositions are distinct from known KREEP basalts (e.g., Figs. 6-8), which suggest long-term depletion of ITE compositions in the mantle sources with low Rb/Sr, high Sm/Nd and Lu/Hf ratios. Such difference between chemical compositions of the CE5 basalts and long-term ITE depleted compositions in mantle source implied by the radiogenic isotopes reflects hybrid components in the mantle sources of CE-5 basalts. Given partition

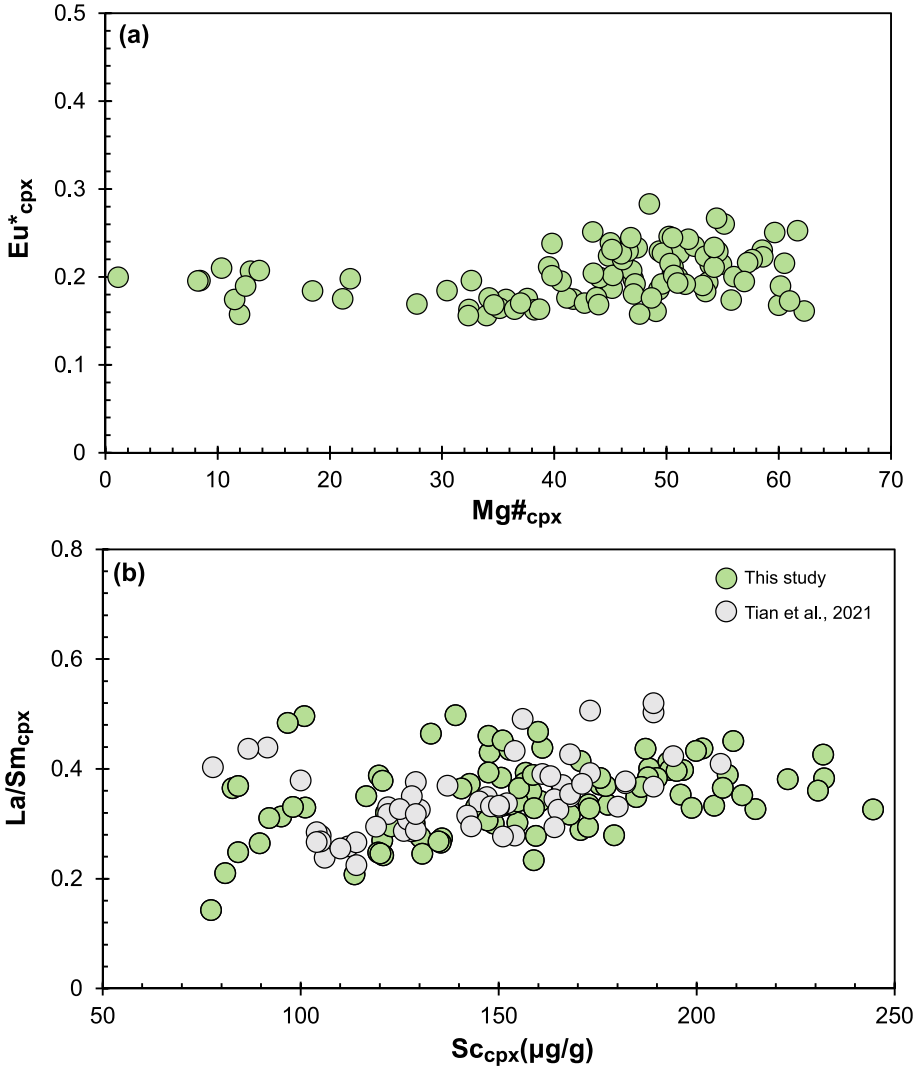

Fig. 9. The Eu* and La/Sm ratio of clinopyroxenes from CE-5 basalts. Clinopyroxenes show variable Mg# and trace element contents but overall constant La/Sm ratio and Eu*. This result reflects limited fractionation of La/Sm and Eu* ratios and also negligible assimilation of KREEP materials during shallow magma fractionation. The data of gray dots are from Tian et al. (2021).

coefficient data (e.g., Dygert et al., 2014; Sun and Liang, 2013), clinopyroxene is the mineral predominant hosting the REE budget in lunar mantle cumulates with low Rb/Sr and high Sm/Nd and Lu/Hf ratios. Clinopyroxene is therefore required to balance the Sr-Nd-Hf isotope composition of the mantle source of the CE-5 basalts which contains a minor KREEP component.

Moreover, as illustrated by the Nb/Ta ratio and Nd-Hf isotopes (Fig. 7d and Fig. 8a), negligible ilmenite was present in the mantle source of CE-5 basalt. However, CE-5 basalts display intermediate TiO_2 content (5–6 wt%, Fig. 4) and its primarily melt likely contains 4.4 wt% TiO_2 (Zhang et al., 2022). Such features also require Ti-rich clinopyroxene in the source. The CE-5 basalt shows affinity to low-Ti basalt, but the Ti#-Fe# relationship of clinopyroxene overlaps with high-Ti basalt rather than low-Ti basalt field (Fig. 8b). Magmatic differentiation cannot account for these features as discussed above. Instead, this indicates the control of source lithology. Titanium is moderately incompatible in clinopyroxene (mostly $D_{Ti} < 0.5$), but Cr is strongly compatible (D_{Cr} often > 5) in this mineral (e.g., Dygert et al., 2014; Leitzke et al., 2016). Residual clinopyroxene in the source would lead to a fractionated Cr/Ti ratio in the melt and would result in the primary melts of CE-5 basalt with high Ti# signature. Therefore, these diverse petrological and geochemical features all strongly indicate clinopyroxene-dominant mantle cumulates with a small fraction of KREEP as the mantle source for the CE-5 basalt.

Pyroxene data, Fe-Mg isotopes, phase diagram and crystallization modelling increasingly support the clinopyroxene-rich cumulate source for CE-5 basalts, although the specific proportion is variable in different studies (Jiang et al., 2023; Luo et al., 2023; Su et al., 2022; Zong et al., 2022). Following previous work (Zong et al., 2022), we modelled this possibility and suggest that 0.5–1.5 modal % KREEP materials would be present in a clinopyroxene-rich (> 30 to 60 molal %) cumulate source of CE-5 basalts (the specific compositions rely on model variables, Fig. 11, see details in Supplementary Materials). Overall, the more clinopyroxene the mantle source contained, the more KREEP would be required. The olivine-bearing pyroxenite mantle source has even been suggested for the CE-5 basalt based on pMELTs simulation and petrological constraints (Luo et al., 2023), implying the possibility of 1–1.5 modal % KREEP in the source of CE-5 basalts.

Because late-stage clinopyroxene crystallized from the lunar magma ocean (i.e., augite) is also rich in TiO_2, FeO and CaO with low Mg# of < 60–70 (Charlier et al., 2018; Elkins-Tanton et al., 2011; Schmidt and Kraettli, 2022; Snyder et al., 1992), we suggest that partial melts of such an augite-rich mantle source with a KREEP flavor can well explain petrological, elemental and isotopic features of the CE-5 basalts (e.g.,

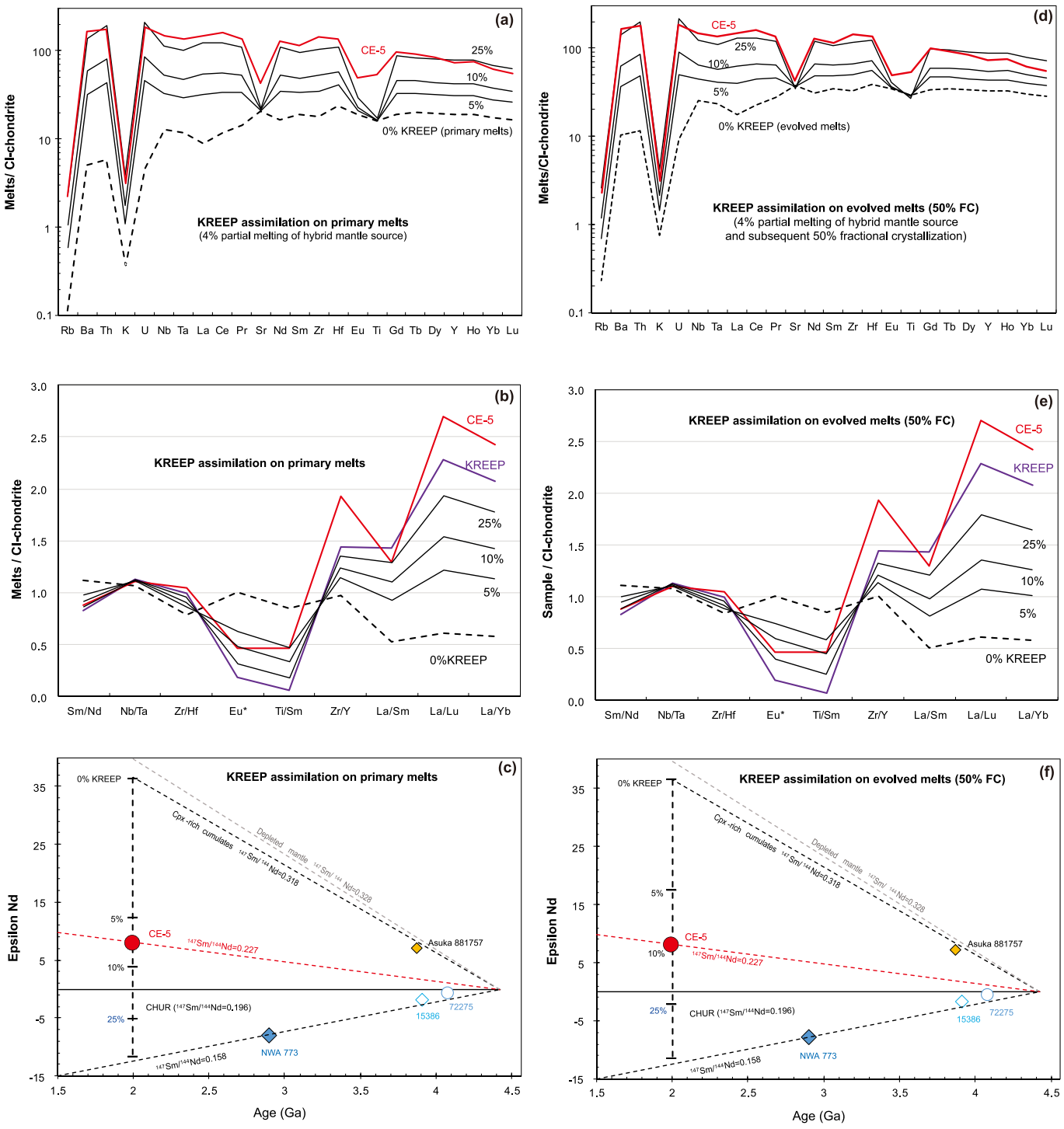

Fig. 10. The modelled effects of assimilation of KREEP materials with ascending primitive (a-c) or evolved melts (d-f, KREEP-melt binary mixing). More than 25% KREEP assimilation is required to replicate the trace elemental contents and ratios, whereas the Nd isotope requires assimilation of only 5–10% KREEP materials. The CHUR, Chondrite Uniform Reservoir. NWA 032, LAP 02205, NWA 4734 are from (Elardo et al., 2014) and references therein. Asuka 881,757 (Misawa et al., 1993), NWA 773 (Borg et al., 2004), 15,386 (Nyquist et al., 1975), 72,275 (Shih et al., 1992) are shown. The estimated depleted lunar mantle is from Elardo et al. (2014).

abundant augite but no orthopyroxene (e.g., Li et al., 2022), high Fe contents, low Mg#, high Ca/Al, high Ti# of clinopyroxene, KREEP property of incompatible trace elements, and overall depleted Sr-Nd-Hf isotopes). The augite accounts for the evolved major element compositions (like low Mg# and high Fe content) and also the depletion in radiogenic Sr-Nd-Hf isotopes (long-term low Rb/Sr, and high Sm/Nd and Lu/Hf ratios in mantle source); whereas the minor interstitial KREEP-like melts explain its main features of patterns and ratios of highly incompatible trace elements (Fig. 11). If its source was rich in calcic ferropyroxene but KREEP-free, as for the YAMM basalts, these trace element compositions and Sr-Nd isotope compositions would be dramatically different (Srivastava et al., 2022). Besides, the low-Mg# (34) feature of CE-5 basalts may also have been partly inherited from low-Mg# augite in the mantle source and may not necessarily reflect high-degree (> 50–70%) fractional crystallization.

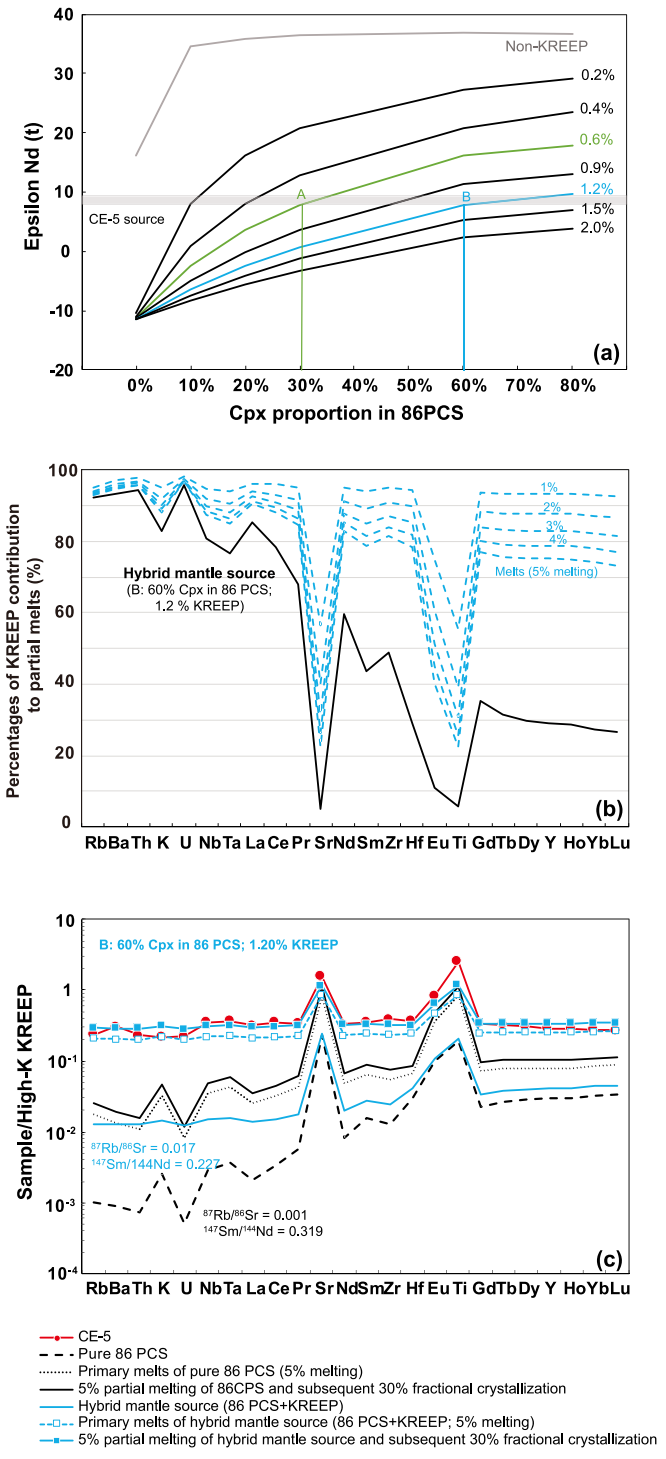

(caption on next column)

Fig. 11. Melting-crystallization modelling of KREEP-bearing, clinopyroxene-rich mantle cumulates to explain KREEP-like trace element patterns and Nd isotopes of CE-5 basalts. (a) Variable proportions of clinopyroxene (0–80%) and high-K KREEP (0–2%) in the mantle sources are calculated to reconcile with ε_{Nd} in the mantle sources of CE-5 basalts. (b) The weight percentages which KREEP component in the hybrid cumulate source contributes to trace element abundances of partial melts after melting. Most of the highly incompatible elements and high-field strength elements are from KREEP components in the hybrid cumulate source; whereas clinopyroxene contributes to most Sr, Eu and Ti to the partial melts. The 4–5% non-modal batch melting of this hybrid mantle source and subsequent 30–50% fractional crystallization can produce a melt with the KREEP-like pattern similar to the CE-5 basalts. These elements in the mantle source, partial melts and evolved melts show patterns or ratios similar to CE-5 basalts (e.g., Sm/Nd, Nb/Ta, Zr/Hf and La/Sm), although the chosen partition coefficients of clinopyroxenes would affect degrees of partial melting and fractional crystallization of clinopyroxenes. Note that the clinopyroxene in the source contributes higher Sr, Ti and Eu proportions to the partial melts relative to neighbouring elements with similar incompatibility, leading to the deviation of Eu*, Rb/Sr and Ti/Sm ratios from high-K KREEP.

The major-element diversity and trace-element pattern uniformity for KREEPy basalts (Warren, 1989; Warren and Wasson, 1979) can be ascribed to the variable distribution of the common last urKREEP dregs of high-degree (> 99%) crystallization of the lunar magma ocean that may then have been remixed in heterogeneous cumulate lithologies after magma ocean overturn (hybrid mantle sources) (Elkins-Tanton et al., 2011). Diverse major elements of KREEP-bearing basalts are likely to reflect different cumulates in their mantle sources, e.g., augite-rich (low Mg#) cumulates for CE-5 basalt but orthopyroxene-rich (high Mg#) source for Apollo 15 KREEP basalts (Ryder, 1987; Taylor et al., 2012). The different proportions of KREEP components in CE-5 basalt and 72,275 (~30% × high-K KREEP) and Apollo 15,386 KREEP basalts (50%-70% × high-K KREEP, Fig. 6 and 7) would result from variable degrees of mantle melting and fractional crystallization, but the KREEP components in their mantle sources overall would be limited (e.g., 1–1.5 modal % for CE-5 basalts and < 5% for 15,386 KREEP, Fig. 11 and S9, and Supplementary Materials).

Because of the additional contribution of mantle cumulate heterogeneity, various types of KREEPy basalts or those with KREEP-like ITE composition (i.e., CE-5 basalt) may display variations in some ITE ratios compared to the urKREEP model composition (e.g., Apollo 15 and 17 KREEP basalts, Fig. 7). Besides a KREEP component, the abundant augite in the CE-5 basalt source would have contributed REE, Ti and other ITE that led to the deviation of Eu* and Ti/Sm ratios from the urKREEP (e.g., Fig. 7 and 11). Because augite-rich cumulates host more Sr and REE relative to orthopyroxene and pigeonite (Dygert et al., 2014; Sun and Liang, 2013), the combined contributions of different magma cumulate lithologies with variably proportions of KREEP components could also explain the different Rb/Sr, Sm/Nd and Lu/Hf ratios (thus variable initial Sr-Nd-Hf isotope compositions) of mantle sources of CE-5 basalts and KREEP basalts.

4.5. *Large-scale, ITE enriched young mare basalts in the PKT*

The CE-5 mission sampled the mare Em4/P58 unit that is composed of distinctive young (~ 2 Ga) moderate-Ti and high-FeO mare basalts. Our laboratory ground-truth compositions confirm their FeO and Ti contents with elevated inherent Th abundance (about 5 μg/g, Fig. 4 and 7, S3). It also reveals a chemically evolved low-Ti mare basalt with KREEP-like ITE signature and its regolith that is overall spatially consistent with the orbital-based remote sensing data of the Em4/P58 unit (e.g., Fu et al., 2021; Jia et al., 2022; Qian et al., 2023). Therefore, the basalts of the Em4/P58 unit (> 1500 km^3), as reflected by CE-5, represent voluminous young volcanism with enriched KREEP-like ITE compositions within mare regions of the northern Oceanus Procellarum (Fig. 1).

Calibration of orbital-based data using CE-5 samples (Liu et al., 2022; Qian et al., 2023) indicates the widespread distribution of young mare basalts with minerals and major elements similar to CE-5 basalts (e.g., abundant augite, moderate Ti and high FeO contents) in the central part of the PKT (orange region in Fig. 1). These young mare basalts suggest that the western PKT is a large region that is underrepresented among the available samples (Prettyman et al., 2006; Qian et al., 2023). Moreover, the unique Apollo 12 basalt fragment 12032,366–18 (Stadermann et al., 2022) and some mare basalts within Mare Imbrium examined by the Chang'e-3 Yutu rover (Ling et al., 2015; Zhang et al., 2015) display mineral and chemical compositions (e.g., high FeO and low Mg# features) consistent with CE-5 basalts (Fig. 4). These young mare basalts likely reflect the widespread presence of clinopyroxene-rich mantle cumulate sources beneath the center area of PKT (Fig. 12). This is consistent with the expected enrichment of low-solidus, high-Ca and high-Fe clinopyroxene (i.e., low-Mg# augite) as late-stage phase of magma ocean evolution (Charlier et al., 2018; Elkins-Tanton et al., 2011; Schmidt and Kraettli, 2022; Snyder et al., 1992) in overturned lunar mantle cumulates.

Importantly, the orbital-based data also have identified high Th and K contents which are widely interpreted to represent the KREEP enrichment of the PKT (Haskin et al., 2000; Jolliff et al., 2000; Lawrence et al., 1998). The CE-5 basalt revealed the existence of basalts in the center of the PKT displaying trace element compositions similar to KREEP, although isotopically they are not KREEPy. The Apollo 12032,366–18 shows a KREEP-rich composition (~0.4 × high-K KREEP) with high Th of 6.9 μg/g, which likely were ejected from Oceanus Procellarum (Stadermann et al., 2022). Consequently, the FeO- and Th-rich young mare basalts in the center of the PKT may be also rich in KREEP-like trace element components and have formed in a similar way as the CE-5 basalts, which would be of great importance for future examination (Fig. 12).

4.6. Implications for the episodic eruption of lunar young mare basalts

The model age distribution of lunar mare basalts shows that basalt magmatism on the Moon was not continuous and that three main episodes occurred at 3.9–3.6 Ga, 3.4–3.0 Ga and 2.2–1.8 Ga (e.g., Hiesinger et al., 2011; Merle et al., 2020; Morota et al., 2011; Qian et al., 2023; Tian et al., 2023b). What mechanisms may have led to these pulses of volcanic activity, and most especially that at 2.2–1.8 Ga, remains unclear. Heating in the lunar interior, such as tidal heating (Che et al., 2021; Harada et al., 2014) or enhanced radioactive elements, seems to be required as an efficient way, although low-solidus characteristics of augite-rich mantle source (e.g., Charlier et al., 2018; Su et al., 2022; Zong et al., 2022) and megaregolith insulation (e.g., Warren et al., 1991;

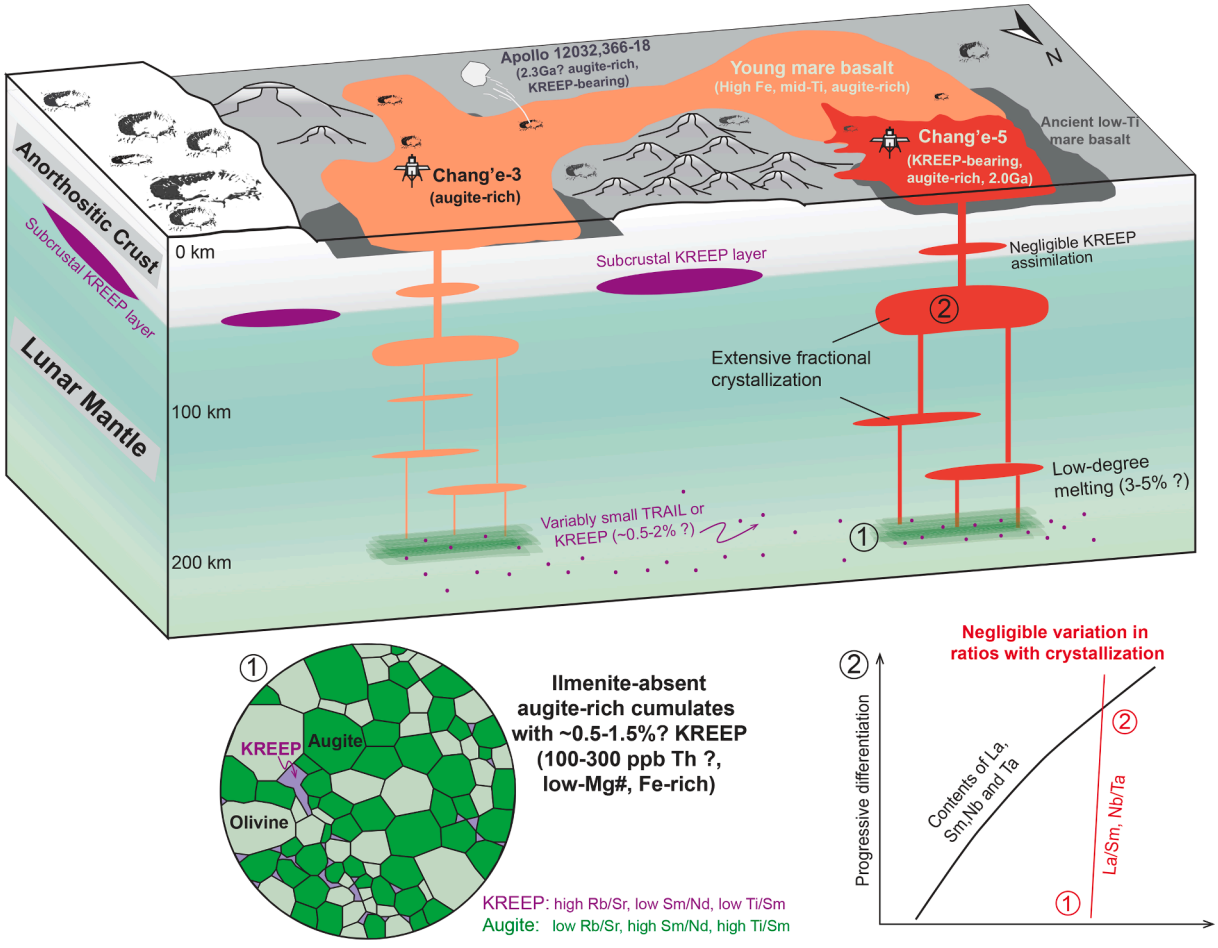

Fig. 12. Schematic cartoon illustrating how augite-rich mantle cumulates with a small distribution of TRAILs or KREEP components produced CE-5 basalt and other large-scale young mare volcanism within the PKT. The CE-5 basalts display abundant augite, low-Mg#, high-Fe and mid-Ti features, as also observed in the basalt fragment 12032,366–18 and Chang'e-3 samples. Impact ejecta from these regions likely delivered 12032,366–18 to the Apollo 12 landing site (Stadermann et al., 2022). The small TRAILs or KREEP components in mantle sources may have promoted melting of augite-rich cumulates via accumulated heat from enhanced radioactive elements such as Th and U. Partial melting and crystallization greatly elevated ITE contents but hardly affected La/Sm, Nb/Ta, Zr/Hf and other ratios of KREEP signatures. Assimilation of any KREEP component occurred during magma ascent was not sufficient to affect the CE-5 basalt's original KREEP-like ITE signature. After eruption at 2.0 Ga, impacts comminuted local basalts to fine particles with limited (<5%) addition of exotic impact ejecta (Zong et al., 2022).

Ziethe et al., 2009) were suggested to facilitate re-melting of source cumulates. A change in depth of source melting may also have been important in the thermal evolution of the Moon (Srivastava et al., 2022).

For 3.4–3.0 Ga magmatism, the urKREEP components in the mantle source were not necessarily present (e.g., Elardo et al., 2014), except the ~ 3.1 Ga KREEP-bearing NWA 773 clan (e.g., Borg et al., 2004; Fagan et al., 2014; Jolliff et al., 2003; Korotev and Irving, 2021). However, their initial Pb isotopic ratios suggest a broad trend towards higher μ-values (reflecting $^{238}U/^{204}Pb$ ratio) in the younger samples (μ from ~300 to ~800 from 3.4 Ga to 3.0 Ga) (e.g., Merle et al., 2020; Snape et al., 2019; Xu et al., 2024). This implies enhanced radioactive elements, which may originate from the widespread trapped interstitial liquid (TRAIL) in overturned mantle cumulates (e.g., Elkins-Tanton et al., 2011; Snyder et al., 1992). The TRAILs are rich in Th and other incompatible elements but do not necessarily have KREEP-like La/Sm, Nb/Ta and Zr/Hf ratios, if they formed earlier than ilmenite separation (e.g., < 95 percent solid) in the evolving LMO (Münker, 2010; Snyder et al., 1992). The amount of TRAIL in mantle sources of mare basalts is typically small, e.g., 1–3 % (e.g., Elkins-Tanton et al., 2011; Hallis et al., 2014; Snyder et al., 1992). The initial Pb isotopic ratio is more sensitive than Nd-Hf isotopes to reflect such enhanced radioactive elements because the former reflects the ratio of highly incompatible U to Pb whereas the latter isotopic ratios are significantly buffered by the mantle cumulates such as clinopyroxene. Both U and Th are highly incompatible and refractory elements, and the Th/U ratio is constant at around 3.7 for diverse types of lunar basalts (Tables S1 and S4) (e.g., Borg et al., 2019; Hallis et al., 2014; Siegler et al., 2022). The initial Pb isotopic ratio (or μ value) is thus a useful indicator for the presence of enhanced radioactive elements including U and Th in mantle sources of lunar basalts.

The CE-5 basalt shows a moderately high μ value of ~ 680 (Che et al., 2021; Li et al., 2021), similar to those of NWA 773 clan and other young low-Ti mare basalts (e.g., Merle et al., 2020; Snape et al., 2019; Xu et al., 2024). The presence of a small quantity of KREEP in the mantle source of CE-5 basalts (e.g., 1–1.5 modal % KREEP) is equivalent to about 200–300 ng/g Th which is noticeably higher than those (e.g., about 50 ng/g Th) used in typical models of the lunar thermal evolution (e.g., Laneuville et al., 2018; Siegler et al., 2022). Therefore, the mantle sources of lunar young mare basalts show some enhanced radioactive element abundances in the form of TRAIL or KREEP components. Based on the orbital high-Th data, it may represent a common scenario in a wide source region of the PKT (Fig. 1). Whether such a level of Th contents had led to the lunar young volcanism needs detailed thermal modelling, which is out of scope of this study. However, here we tentatively propose a conceptual model to explain the interval eruption of the lunar late-stage mare basalts for future consideration.

In general, a gradual heat production via time-related radiogenic decay or tidal heating (Che et al., 2021; Harada et al., 2014) competes with the thickening lunar lithosphere and megaregolith with secular cooling and impacts on the surface (i.e., the thermal lid for heat insulation) (e.g., Head and Wilson, 2017; Hiesinger and Head, 2006; Ziethe et al., 2009). If there was no internal heating, it would be difficult for the solidified lunar mantle cumulates to remelt; whereas if the Th or U contents were too high, then lunar basalt eruption would be expected to be continuous rather than episodic. Instead, a moderate amount of radioactive elements (e.g., 200–300 ng/g Th for CE-5) may be required. The heat accumulated at early stages was lower than the dissipated heat when the lithosphere and porous crust were thin (i.e., neither melting nor eruption). However, with secular cooling and thickening of the lunar lithosphere and megaregolith, the heat became accumulated until it reached the melting point of cumulate sources (i.e., eruption occurs). This model, if confirmed, may explain the high melting temperature beneath some PKT regions (e.g., 1350 ± 50°C for the mantle source of CE-5 basalt) (Luo et al., 2023). The variably dispersed distribution of TRAIL or KREEP components (thus enhanced radioactive elements) within lunar mantle cumulates could be a reasonable mechanism for the lunar young volcanism, and also reconcile with other geophysical observations of the high electrical conductivity (Grimm, 2013), low magnetic field intensity (Wieczorek, 2018) and negative topography anomaly within the Procellarum KREEP Terrane (Andrews-Hanna et al., 2014).

5. Conclusions

The CE-5 scooped and drilled soils show a remarkable homogeneity in chemical composition at the milligram level, and the ratios of highly incompatible elements are similar to those of basalt clasts (such as La/Sm and Nb/Ta), indicating that the CE-5 soil formed mainly (> 95%) from the local basalt of the Em5/P58 unit. Its spatial distribution in the mare region of the Em4/P58 unit, petrological and geochemical features (e.g., Nd-Hf isotope correlation) reflect its affinity to low-Ti mare basalt; whereas it also displays high concentrations of incompatible trace elements (~ 0.3 × high-K KREEP; ~5.1 μg/g Th) with KREEP-like ITE compositions. Such KREEP-like components are difficult to explain by exotic impact ejecta, magma differentiation or significant assimilation of KREEP materials during magma eruption, and must be inherited from its mantle source. The absence of noticeable assimilation of KREEP components likely suggests a lack of a kilometer-thick subcrustal KREEP layer, at least in the Em4/P58 unit. The CE-5 basalt is thus a chemically evolved low-Ti mare basalt with enhanced KREEP-like ITE but isotopically depleted Nd and Hf isotope compositions, which has not been previously recognized in available lunar samples. We propose that the mantle source of CE-5 basalt was ilmenite-absent, KREEP-bearing (~ 1–1.5 modal %, equivalent to 200–300 ng/g Th) and contained abundant (> 30–60%) augite cumulates from the late stages of crystallization of the lunar magma ocean. Low-degree partial melting and subsequent fractional crystallization significantly enhanced incompatible element concentrations to ~ 0.3 × KREEP.

The mare basalts in the Em4/P58 unit thus reveal large-scale, ITE enriched young mare volcanism within Oceanus Procellarum and augite-rich mantle cumulate with variably dispersed small KREEP components as a key ingredient for lunar young volcanism. According to the remote sensing data and the unique Apollo 12 basalt fragment 12032,366–18, a large part of FeO- and Th-rich mare regions at the center of PKT may have formed in a way similar to the CE-5 basalt. The initial Pb isotope compositions indicate a broad trend towards higher μ-values (600–800) and thus enhanced radioactive elements in the mantle sources of the young low-Ti basalts (including those erupted around 3.0 Ga), which may be related to a small amount of trapped interstitial liquids (TRAIL) or KREEP components. Whether such enhanced radioactive elements can explain the episodic eruption of lunar young mare volcanism requires detailed thermal modelling.

Data availability

Data are available through Mendeley Data: https://doi.org/10.17632/k2jhvmkmy6.1.

CRediT authorship contribution statement

Zaicong Wang: Writing – review & editing, Writing – original draft, Methodology, Investigation, Funding acquisition, Formal analysis, Data curation, Conceptualization. **Keqing Zong:** Writing – review & editing, Writing – original draft, Formal analysis, Data curation, Conceptualization. **Yiheng Li:** Writing – original draft, Formal analysis, Conceptualization. **Jiawei Li:** Formal analysis. **Qi He:** Resources. **Zongqi Zou:** Writing – original draft, Methodology, Investigation, Formal analysis, Data curation. **Harry Becker:** Supervision, Conceptualization. **Frédéric Moynier:** Supervision. **James M.D. Day:** Writing – review & editing, Supervision, Conceptualization. **Wen Zhang:** Formal analysis, Data curation. **Yuqi Qian:** Investigation. **Long Xiao:** Resources, Investigation. **Zhaochu Hu:** Resources. **Zhenbing She:** Resources. **Hejiu Hui:**

Supervision, Conceptualization. **Xiang Wu:** Resources. **Yongsheng Liu:** Resources.

Declaration of competing interest

The authors declare that they have no known competing financial interests or personal relationships that could have appeared to influence the work reported in this paper.

Acknowledgments

We thank Marc Norman, Stephen Elardo and the anonymous reviewers for constructive comments that have greatly improved the quality of the manuscript. Janne Blichert-Toft is also thanked for her comments and efficient editorial handling. We appreciate all staff of the Chang'e-5 mission for returning samples and the China National Space Administration (CNSA) for providing samples (CE5C0400, CE5Z0204YJ, and CE5Z0906YJ). This work was supported by the National Natural Science Foundation of China (No. 42241156), the pre-research project on Civil Aerospace Technologies funded by CNSA (No. D020205), and the outstanding youth team project of China University of Geosciences, Wuhan (G1323523042). We thank Xiaohui Fu for providing remote sensing data and Yun Jiang for insightful discussion and colleagues at the State Key Laboratory of Geological Processes and Mineral Resources (CUG Wuhan) for great technique support.

Appendix A. Supplementary material

This supplementary material includes: 1) Partial melting and fractional crystallization modelling of hybrid mantle sources. 2) Melting and fractionation models for CE-5 basalt. 3) Effects of models and partition coefficients. 4) Variable mantle lithology for lunar KREEP basalts. 5) Supplementary figures and tables. The Tables S1-6 are presented in a separate Excel file in online Mendeley database. Supplementary material to this article can be found online at https://doi.org/10.1016/j.gca.2024.03.029.

References

Andrews-Hanna, J.C., Besserer, J., Head Iii, J.W., Howett, C.J.A., Kiefer, W.S., Lucey, P. J., McGovern, P.J., Melosh, H.J., Neumann, G.A., Phillips, R.J., Schenk, P.M., Smith, D.E., Solomon, S.C., Zuber, M.T., 2014. Structure and evolution of the lunar Procellarum region as revealed by GRAIL gravity data. Nature 514, 68–71.

Arai, T., Warren, P.H., Takeda, H., 1996. Four lunar mare meteorites: crystallization trends of pyroxenes and spinels. Meteorit. Planet. Sci. 31, 877–892.

Beard, B.L., Taylor, L.A., Scherer, E.E., Johnson, C.M., Snyder, G.A., 1998. The source region and melting mineralogy of high-titanium and low-titanium lunar basalts deduced from Lu-Hf isotope data. Geochim. Cosmochim. Acta 62, 525–544.

Borg, L.E., Carlson, R.W., 2023. The evolving chronology of moon formation. Annu. Rev. Earth Planet. 51, 25–52.

Borg, L.E., Shearer, C.K., Asmerom, Y., Papike, J.J., 2004. Prolonged KREEP magmatism on the moon indicated by the youngest dated lunar igneous rock. Nature 432, 209–211.

Borg, L.E., Gaffney, A.M., Shearer, C.K., DePaolo, D.J., Hutcheon, I.D., Owens, T.L., Ramon, E., Brennecka, G., 2009. Mechanisms for incompatible-element enrichment on the moon deduced from the lunar basaltic meteorite Northwest Africa 032. Geochim. Cosmochim. Acta 73, 3963–3980.

Borg, L.E., Gaffney, A.M., Kruijer, T.S., Marks, N.A., Sio, C.K., Wimpenny, J., 2019. Isotopic evidence for a young lunar magma ocean. Earth Planet. Sci. Lett. 523, 115706.

Cao, K., Dong, M., She, Z., Xiao, Q., Wang, X., Qian, Y., Li, Y., Wang, Z., He, Q., Wu, X., Zong, K., Hu, Z., Xiao, L., 2022. A novel method for simultaneous analysis of particle size and mineralogy for Chang'E-5 lunar soil with minimum sample consumption. Sci. China Earth Sci. 65, 1704–1714.

Charlier, B., Grove, T.L., Namur, O., Holtz, F., 2018. Crystallization of the lunar magma ocean and the primordial mantle-crust differentiation of the moon. Geochim. Cosmochim. Acta 234, 50–69.

Che, X., Nemchin, A., Liu, D., Long, T., Wang, C., Norman, M.D., Joy, K.H., Tartese, R., Head, J., Jolliff, B., Snape, J.F., Neal, C.R., Whitehouse, M.J., Crow, C., Benedix, G., Jourdan, F., Yang, Z., Yang, C., Liu, J., Xie, S., Bao, Z., Fan, R., Li, D., Li, Z., Webb, S. G., 2021. Age and composition of young basalts on the moon, measured from samples returned by chang'e-5. Science 374, 887–890.

Chen, Y., Hu, S., Li, J.-H., Li, Q.-L., Li, X., Li, Y., Liu, Y., Qian, Y., Yang, W., Zhou, Q., Lin, Y., Li, C., Li, X.-H., 2023. Chang'e-5 lunar samples shed new light on the moon. The Innovation Geoscience 1, 100014.

Day, J.M.D., 2020. Metal grains in lunar rocks as indicators of igneous and impact processes. Meteorit. Planet. Sci. 55, 1793–1807.

Day, J.M.D., Taylor, L.A., Floss, C., Patchen, A.D., Schnare, D.W., Pearson, D.G., 2006. Comparative petrology, geochemistry, and petrogenesis of evolved, low-Ti lunar mare basalt meteorites from the LaPaz icefield Antarctica. Geochim. Cosmochim. Acta 70, 1581–1600.

Du, J., Fa, W., Gong, S., Liu, Y., Qiao, L., Tai, Y., Zhang, F., Zou, Y., 2022. Thicknesses of mare basalts in the Chang'E-5 landing region: implications for the late-stage volcanism on the moon. J. Geophys. Res. Planets 127, e2022JE007314.

Dygert, N., Liang, Y., Sun, C., Hess, P., 2014. An experimental study of trace element partitioning between augite and Fe-rich basalts. Geochim. Cosmochim. Acta 132, 170–186.

Dygert, N., Draper, D.S., Rapp, J.F., Lapen, T.J., Fagan, A.L., Neal, C.R., 2020. Experimental determinations of trace element partitioning between plagioclase, pigeonite, olivine, and lunar basaltic melts and an fO2 dependent model for plagioclase-melt Eu partitioning. Geochim. Cosmochim. Acta 279, 258–280.

Elardo, S.M., Shearer Jr., C.K., Fagan, A.L., Borg, L.E., Gaffney, A.M., Burger, P.V., Neal, C.R., Fernandes, V.A., McCubbin, F.M., 2014. The origin of young mare basalts inferred from lunar meteorites Northwest Africa 4734, 032, and LaPaz icefield 02205. Meteorit. Planet. Sci. 49, 261–291.

Elkins-Tanton, L.T., Burgess, S., Yin, Q.-Z., 2011. The lunar magma ocean: reconciling the solidification process with lunar petrology and geochronology. Earth Planet. Sci. Lett. 304, 326–336.

Fagan, T.J., Kashima, D., Wakabayashi, Y., Suginohara, A., 2014. Case study of magmatic differentiation trends on the moon based on lunar meteorite Northwest Africa 773 and comparison with apollo 15 quartz monzodiorite. Geochim. Cosmochim. Acta 133, 97–127.

Fu, X., Hou, X., Zhang, J., Li, B., Ling, Z., Jolliff, B.L., Xu, L., Zou, Y., 2021. Possible non-mare lithologies in the regolith at the Chang'E-5 landing site: evidence from remote sensing data. J. Geophys. Res. Planets 126, e2020JE006797.

Fu, X., Yin, C., Jolliff, B.L., Zhang, J., Chen, J., Ling, Z., Zhang, F., Liu, Y., Zou, Y., 2022. Understanding the mineralogy and geochemistry of Chang'E-5 soil and implications for its geological significances. Icarus 388, 115254.

Gaffney, A.M., Borg, L.E., 2014. A young solidification age for the lunar magma ocean. Geochim. Cosmochim. Acta 140, 227–240.

Grimm, R.E., 2013. Geophysical constraints on the lunar Procellarum KREEP terrane. J. Geophys. Res. Planets 118, 768–778.

Hallis, L.J., Anand, M., Strekopytov, S., 2014. Trace-element modelling of mare basalt parental melts: implications for a heterogeneous lunar mantle. Geochim. Cosmochim. Acta 134, 289–316.

Harada, Y., Goossens, S., Matsumoto, K., Yan, J., Ping, J., Noda, H., Haruyama, J., 2014. Strong tidal heating in an ultralow-viscosity zone at the core–mantle boundary of the moon. Nat. Geosci. 7, 569–572.

Haskin, L.A., 1998. The imbrium impact event and the thorium distribution at the lunar highlands surface. J. Geophys. Res. Planets 103, 1679–1689.

Haskin, L.A., Gillis, J.J., Korotev, R.L., Jolliff, B.L., 2000. The materials of the lunar Procellarum KREEP terrane: a synthesis of data from geomorphological mapping, remote sensing, and sample analyses. J. Geophys. Res. Planets 105, 20403–20415.

He, Q., Li, Y., Baziotis, I., Qian, Y., Xiao, L., Wang, Z., Zhang, W., Luo, B., Neal, C.R., Day, J.M.D., Pan, F., She, Z., Wu, X., Hu, Z., Zong, K., Wang, L., 2022. Detailed petrogenesis of the unsampled oceanus Procellarum: the case of the chang'e-5 mare basalts. Icarus 383, 115082.

Head, J.W., Wilson, L., 2017. Generation, ascent and eruption of magma on the moon: new insights into source depths, magma supply, intrusions and effusive/explosive eruptions (Part 2: predicted emplacement processes and observations). Icarus 283, 176–223.

Hess, P.C., Parmentier, E.M., 2001. Thermal evolution of a thicker KREEP liquid layer. J. Geophys. Res. Planets 106, 28023–28032.

Hiesinger, H., Head, J.W., III, Wolf, U., Jaumann, R., Neukum, G., Ambrose, W.A. and Williams, D.A. (2011) Ages and stratigraphy of lunar mare basalts: A synthesis, in: Ambrose, W.A., Williams, D.A. (Eds.), Recent Advances and Current Research Issues in Lunar Stratigraphy. Geological Society of America, pp. 1-51.

Hiesinger, H., Head, J., 2006. New views of lunar geoscience: an introduction and overview. Rev. Mineral. Geochem. 60, 1–81.

Hu, Z., Gao, S., Liu, Y., Hu, S., Chen, H., Yuan, H., 2008. Signal enhancement in laser ablation ICP-MS by addition of nitrogen in the central channel gas. J. Anal. At. Spectrom 23, 1093–1101.

Hui, H., Neal, C.R., Shih, C.-Y., Nyquist, L.E., 2013. Petrogenetic association of the oldest lunar basalts: combined Rb–Sr isotopic and trace element constraints. Earth Planet. Sci. Lett. 373, 150–159.

Jia, B., Fa, W., Xie, M., Tai, Y., Liu, X., 2021. Regolith properties in the Chang'E-5 landing region of the moon: results from multi-source remote sensing observations. J. Geophys. Res. Planets 126, e2021JE006934.

Jia, B., Fa, W., Zhang, M., Di, K., Xie, M., Tai, Y., Li, Y., 2022. On the provenance of the Chang'E-5 lunar samples. Earth Planet. Sci. Lett. 596, 117791.

Jiang, Y., Li, Y., Liao, S., Yin, Z., Hsu, W., 2022. Mineral chemistry and 3D tomography of a chang'e 5 high-ti basalt: implication for the lunar thermal evolution history. Science Bulletin 67, 755–761.

Jiang, Y., Kang, J., Liao, S., Elardo, S.M., Zong, K., Wang, S., Nie, C., Li, P., Yin, Z., Huang, F., Hsu, W., 2023. Fe and mg isotope compositions indicate a hybrid mantle source for young chang'e 5 Mare basalts. The Astrophysical Journal Letters 945, L26.

Jolliff, B.L., Gillis, J.J., Haskin, L.A., Korotev, R.L., Wieczorek, M.A., 2000. Major lunar crustal terranes: surface expressions and crust-mantle origins. J. Geophys. Res. Planets 105, 4197–4216.
Jolliff, B.L., Korotev, R.L., Zeigler, R.A., Floss, C., 2003. Northwest Africa 773: lunar mare breccia with a shallow-formed olivine-cumulate component, inferred very-low-ti (VLT) heritage, and a KREEP connection. Geochim. Cosmochim. Acta 67, 4857–4879.
Korotev, R.L., 2005. Lunar geochemistry as told by lunar meteorites. Geochemistry 65, 297–346.
Korotev, R.L., Irving, A.J., 2021. Lunar meteorites from northern Africa. Meteorit. Planet. Sci. 56, 206–240.
Laneuville, M., Wieczorek, M.A., Breuer, D., Tosi, N., 2013. Asymmetric thermal evolution of the moon. J. Geophys. Res. Planets 118, 1435–1452.
Laneuville, M., Taylor, J., Wieczorek, M.A., 2018. Distribution of radioactive heat sources and thermal history of the moon. J. Geophys. Res. Planets 123, 3144–3166.
Lawrence, D.J., Feldman, W.C., Barraclough, B.L., Binder, A.B., Elphic, R.C., Maurice, S., Thomsen, D.R., 1998. Global elemental maps of the moon: the Lunar prospector gamma-ray spectrometer. Science 281, 1484–1489.
Leitzke, F.P., Fonseca, R.O.C., Michely, L.T., Sprung, P., Münker, C., Heuser, A., Blanchard, H., 2016. The effect of titanium on the partitioning behavior of high-field strength elements between silicates, oxides and lunar basaltic melts with applications to the origin of mare basalts. Chem. Geol. 440, 219–238.
Li, C., Hu, H., Yang, M.-F., Pei, Z.-Y., Zhou, Q., Ren, X., Liu, B., Liu, D., Zeng, X., Zhang, G., Zhang, H., Liu, J., Wang, Q., Deng, X., Xiao, C., Yao, Y., Xue, D., Zuo, W., Su, Y., Wen, W., Ouyang, Z., 2022. Characteristics of the lunar samples returned by the Chang'E-5 mission. Nat. Sci. Rev. 9, nwab188.
Li, Y., Wang, Z., Zhang, W., Zhou, L., Zong, K., Feng, L., Li, J., He, Q., She, Z., Wu, X., Hu, Z., Xiao, L., Wu, Y., Liu, Y., 2023. Rb-sr isotopes record complex thermal modification of chang'e-5 lunar soils. Science Bulletin 68, 2724–2728.
Li, Q.-L., Zhou, Q., Liu, Y., Xiao, Z., Lin, Y., Li, J.-H., Ma, H.-X., Tang, G.-Q., Guo, S., Tang, X., Yuan, J.-Y., Li, J., Wu, F.-Y., Ouyang, Z., Li, C., Li, X.-H., 2021. Two-billion-year-old volcanism on the moon from chang'e-5 basalts. Nature 600, 54–58.
Lin, R., Lin, J., Zong, K., Chen, K., Tong, S., Feng, L., Zhang, W., Li, M., Liu, Y., Hu, Z., Zhou, L., 2020. Determination of the isotopic composition of an enriched hafnium spike by MC-ICP-MS using a regression model. Geostand. Geoanal. Res. 44, 753–762.
Ling, Z., Jolliff, B.L., Wang, A., Li, C., Liu, J., Zhang, J., Li, B., Sun, L., Chen, J., Xiao, L., Liu, J., Ren, X., Peng, W., Wang, H., Cui, X., He, Z., Wang, J., 2015. Correlated compositional and mineralogical investigations at the chang'e-3 landing site. Nat. Commun. 6, 8880.
Liu, Y.S., Hu, Z.C., Gao, S., Gunther, D., Xu, J., Gao, C.G., Chen, H.H., 2008. In situ analysis of major and trace elements of anhydrous minerals by LA-ICP-MS without applying an internal standard. Chem. Geol. 257, 34–43.
Liu, D., Wang, X., Liu, J., Liu, B., Ren, X., Chen, Y., Chen, Z., Zhang, H., Zhang, G., Zhou, Q., Zhang, Z., Fu, Q., Li, C., 2022. Spectral interpretation of late-stage mare basalt mineralogy unveiled by Chang'E-5 samples. Nat. Commun. 13, 5965.
Long, T., Qian, Y., Norman, M.D., Miljkovic, K., Crow, C., Head, J.W., Che, X., Tartèse, R., Zellner, N., Yu, X., Xie, S., Whitehouse, M., Joy, K.H., Neal, C.R., Snape, J.F., Zhou, G., Liu, S., Yang, C., Yang, Z., Wang, C., Xiao, L., Liu, D., Nemchin, A., 2022. Constraining the formation and transport of lunar impact glasses using the ages and chemical compositions of Chang'e 5 glass beads. Sci. Adv. 8, eabq2542.
Luo, B., Wang, Z., Song, J., Qian, Y., He, Q., Li, Y., Head, J.W., Moynier, F., Xiao, L., Becker, H., Huang, B., Ruan, B., Hu, Y., Pan, F., Xu, C., Liu, W., Zong, K., Zhao, J., Zhang, W., Hu, Z., She, Z., Wu, X., Zhang, H., 2023. The magmatic architecture and evolution of the chang'e-5 lunar basalts. Nat. Geosci. 7, 287–297.
McKay, G., Wiesmann, H., Nyquist, L., Wooden, J., Bansal, B., 1978. Petrology, chemistry, and chronology of 14078-chemical constraints on the origin of KREEP. Lunar and Planetary Science Conference Proceedings 661–687.
Mei, A., Jiang, Y., Liao, S., Kang, J., Huang, F., Hsu, W., 2023. KREEP-rich breccia in Chang'E-5 regolith and its implications. Sci. China Earth Sci. 66, 2473–2486.
Merle, R.E., Nemchin, A.A., Whitehouse, M.J., Snape, J.F., Kenny, G.G., Bellucci, J.J., Connelly, J.N., Bizzarro, M., 2020. Pb-pb ages and initial pb isotopic composition of lunar meteorites: NWA 773 clan, NWA 4734, and Dhofar 287. Meteorit. Planet. Sci. 55, 1808–1832.
Misawa, K., Tatsumoto, M., Dalrymple, G.B., Yanai, K., 1993. An extremely low U/Pb source in the moon: U-Th-Pb, Sm-Nd, Rb-Sr, and $^{40}Ar/^{39}Ar$ isotopic systematics and age of lunar meteorite asuka 881757. Geochim. Cosmochim. Acta 57, 4687–4702.
Morota, T., Haruyama, J., Ohtake, M., Matsunaga, T., Honda, C., Yokota, Y., Kimura, J., Ogawa, Y., Hirata, N., Demura, H., Iwasaki, A., Sugihara, T., Saiki, K., Nakamura, R., Kobayashi, S., Ishihara, Y., Takeda, H., Hiesinger, H., 2011. Timing and characteristics of the latest mare eruption on the moon. Earth Planet. Sci. Lett. 302, 255–266.
Münker, C., 2010. A high field strength element perspective on early lunar differentiation. Geochim. Cosmochim. Acta 74, 7340–7361.
Neal, C.R., 2001. Interior of the moon: the presence of garnet in the primitive deep lunar mantle. J. Geophys. Res. Planets 106, 27865–27885.
Neal, C.R., Kramer, G.Y., 2006. The petrogenesis of the apollo 14 high-Al mare basalts. Am. Mineral. 91, 1521–1535.
Neal, C.R., Taylor, L.A., 1992. Petrogenesis of mare basalts: a record of lunar volcanism. Geochim. Cosmochim. Acta 56, 2177–2211.
Nyquist, L., Bansal, B., Wiesmann, H., 1975. Rb-sr ages and initial sr-87/Sr-86 for apollo 17 basalts and KREEP basalt 15386. Lunar and Planetary Science Conference Proceedings 1445–1465.
Nyquist, L.E., Shih, C.Y., 1992. The isotopic record of lunar volcanism. Geochim. Cosmochim. Acta 56, 2213–2234.
Papike, J.J., Hodges, F.N., Bence, A.E., Cameron, M., Rhodes, J.M., 1976. Mare basalts: crystal chemistry, mineralogy, and petrology. Rev. Geophys. 14, 475–540.
Prettyman, T.H., Hagerty, J.J., Elphic, R.C., Feldman, W.C., Lawrence, D.J., McKinney, G.W., Vaniman, D.T., 2006. Elemental composition of the lunar surface: analysis of gamma ray spectroscopy data from Lunar prospector. J. Geophys. Res. Planets 111.
Qian, Y., Xiao, L., Head, J.W., van der Bogert, C.H., Hiesinger, H., Wilson, L., 2021. Young lunar mare basalts in the chang'e-5 sample return region, northern oceanus procellarum. Earth Planet. Sci. Lett. 555, 116702.
Qian, Y., She, Z., He, Q., Xiao, L., Wang, Z., Head, J.W., Sun, L., Wang, Y., Wu, B., Wu, X., Luo, B., Cao, K., Li, Y., Dong, M., Song, W., Pan, F., Michalski, J., Ye, B., Zhao, J., Zhao, S., Huang, J., Zhao, J., Wang, J., Zong, K., Hu, Z., 2023. Mineralogy and chronology of the young mare volcanism in the procellarum-KREEP-terrane. Nat. Astron. 7, 287–297.
Robinson, K.L., Treiman, A.H., Joy, K.H., 2012. Basaltic fragments in lunar feldspathic meteorites: connecting sample analyses to orbital remote sensing. Meteorit. Planet. Sci. 47, 387–399.
Ryder, G., 1987. Petrographic evidence for nonlinear cooling rates and a volcanic origin for apollo 15 KREEP basalts. J. Geophys. Res. Solid Earth 92, E331–E339.
Ryder, G., Stoeser, D.B., Wood, J.A., 1977. Apollo 17 KREEPy basalt: a rock type intermediate between mare and KREEP basalts. Earth Planet. Sci. Lett. 35, 1–13.
Salpas, P.A., Taylor, L.A., Lindstrom, M.M., 1987. Apollo 17 KREEPy basalts: evidence for nonuniformity of KREEP. J. Geophys. Res. Solid Earth 92, E340–E348.
Schmidt, M.W., Kraettli, G., 2022. Experimental crystallization of the lunar magma ocean, initial selenotherm and density stratification, and implications for crust formation, overturn and the bulk silicate moon composition. J. Geophys. Res. Planets 127, e2022JE007187.
Shearer, C.K., Hess, P.C., Wieczorek, M.A., Pritchard, M.E., Parmentier, E.M., Borg, L.E., Longhi, J., Elkins-Tanton, L.T., Neal, C.R., Antonenko, I., Canup, R.M., Halliday, A. N., Grove, T.L., Hager, B.H., Lee, D.C., Wiechert, U., 2006. Thermal and magmatic evolution of the moon. In: Jolliff, B.L., Wieczorek, M.A. (Eds.), New Views of the Moon. Mineralogical Soc Amer & Geochemical Soc, Chantilly, pp. 365–518.
Shih, C.Y., Nyquist, L.E., Bansal, B.M., Wiesmann, H., 1992. Rb-sr and sm-nd chronology of an apollo 17 KREEP basalt. Earth Planet. Sci. Lett. 108, 203–215.
Siegler, M., Warren, P., Franco, K.L., Paige, D., Feng, J., White, M., 2022. Lunar heat flow: global predictions and reduced heat flux. J. Geophys. Res. Planets 127, e2022JE007182.
Snape, J.F., Nemchin, A.A., Whitehouse, M.J., Merle, R.E., Hopkinson, T., Anand, M., 2019. The timing of basaltic volcanism at the apollo landing sites. Geochim. Cosmochim. Acta 266, 29–53.
Snyder, G.A., Taylor, L.A., Neal, C.R., 1992. A chemical model for generating the sources of mare basalts: combined equilibrium and fractional crystallization of the lunar magmasphere. Geochim. Cosmochim. Acta 56, 3809–3823.
Sprung, P., Kleine, T., Scherer, E.E., 2013. Isotopic evidence for chondritic Lu/Hf and Sm/Nd of the moon. Earth Planet. Sci. Lett. 380, 77–87.
Srivastava, Y., Basu Sarbadhikari, A., Day, J.M.D., Yamaguchi, A., Takenouchi, A., 2022. A changing thermal regime revealed from shallow to deep basalt source melting in the moon. Nat. Commun. 13, 7594.
Stadermann, A.C., Jolliff, B.L., Krawczynski, M.J., Hamilton, C.W., Barnes, J.J., 2022. Analysis and experimental investigation of apollo sample 12032,366–18, a chemically evolved basalt from the moon. Meteorit. Planet. Sci. 57, 794–816.
Su, B., Yuan, J., Chen, Y., Yang, W., Mitchell, R.N., Hui, H., Wang, H., Tian, H., Li, X.-H., Wu, F.-Y., 2022. Fusible mantle cumulates trigger young mare volcanism on the cooling moon. Sci. Adv. 8, eabn2103.
Sun, C., Liang, Y., 2013. Distribution of REE and HFSE between low-Ca pyroxene and lunar picritic melts around multiple saturation points. Geochim. Cosmochim. Acta 119, 340–358.
Taylor, G.J., Martel, L.M.V., Spudis, P.D., 2012. The Hadley-apennine KREEP basalt igneous province. Meteorit. Planet. Sci. 47, 861–879.
Tian, H.-C., Wang, H., Chen, Y., Yang, W., Zhou, Q., Zhang, C., Lin, H.-L., Huang, C., Wu, S.-T., Jia, L.-H., Xu, L., Zhang, D., Li, X.-G., Chang, R., Yang, Y.-H., Xie, L.-W., Zhang, D.-P., Zhang, G.-L., Yang, S.-H., Wu, F.-Y., 2021. Non-KREEP origin for Chang'E-5 basalts in the procellarum KREEP terrane. Nature 600, 59–63.
Tian, H.-C., Yang, W., Zhang, D., Zhang, H., Jia, L., Wu, S., Lin, Y., Li, X., Wu, F., 2022. Petrogenesis of Chang'E-5 mare basalts: clues from the trace elements in plagioclase. Am. Mineral.
Tian, H.-C., Yang, W., Gao, Y., Zhou, Q., Ruan, R., Lin, Y., Li, X., Wu, F., 2023a. Reassessing the classification of chang'e-5 basalts using pyroxene composition. Lithos 456–457, 107309.
Tian, H.-C., Zhang, C., Yang, W., Du, J., Chen, Y., Xiao, Z., Mitchell, R.N., Hui, H., Changela, H.G., Zhang, T.-X., Tang, X., Zhang, D., Lin, Y., Li, X., Wu, F., 2023b. Surges in volcanic activity on the moon about two billion years ago. Nat. Commun. 14, 3734.
Unruh, D.M., Stille, P., Patchett, P.J., Tatsumoto, M., 1984. Lu-Hf and Sm-Nd evolution in lunar mare basalts. J. Geophys. Res. Solid Earth 89, B459–B477.
Wang, Z., Wang, W., Tian, W., Li, H., Qian, Y., Pei, J., Chen, Z., Wang, D., Liu, P.-P., Fa, W., Wu, J., Bao, H., 2023. Cooling rate of clinopyroxene reveals the thickness and effusion volume of Chang'E-5 basaltic flow units. Icarus 394, 115406.
Warren, P.H., Haack, H., Rasmussen, K.L., 1991. Megaregolith insulation and the duration of cooling to isotopic closure within differentiated asteroids and the moon. J. Geophys. Res. Solid Earth 96, 5909–5923.
Warren, P.H., Wasson, J.T., 1979. The origin of KREEP. Rev. Geophys. 17, 73–88.
Warren, P.H. (1989) KREEP: Major-Element Diversity, Trace-Element Uniformity (Almost), Moon in Transition: Apollo 14, KREEP, and Evolved Lunar Rocks, pp. 149-153.

Wieczorek, M.A., 2018. Strength, depth, and geometry of magnetic sources in the crust of the moon from localized power Spectrum analysis. J. Geophys. Res. Planets 123, 291–316.
Wieczorek, M.A., Jolliff, B.L., Khan, A., Pritchard, M.E., Weiss, B.P., Williams, J.G., Hood, L.L., Righter, K., Neal, C.R., Shearer, C.K., McCallum, I.S., Tompkins, S., Hawke, B.R., Peterson, C., Gillis, J.J., Bussey, B., 2006. The constitution and structure of the lunar interior. In: Jolliff, B.L., Wieczorek, M.A. (Eds.), New Views of the Moon. Mineralogical Soc Amer & Geochemical Soc, Chantilly, pp. 221–364.
Wieczorek, M.A., Phillips, R.J., 2000. The "procellarum KREEP terrane": implications for mare volcanism and lunar evolution. J. Geophys. Res. Planets 105, 20417–20430.
Xu, J.-Y., Li, Q.-L., Lu, K., Li, X.-H., 2024. Chang'e-5 basalt-like non-KREEP young lunar meteorite. Science Bulletin 69, 601–605.
Yang, W., Chen, Y., Wang, H., Tian, H.-C., Hui, H., Xiao, Z., Wu, S.-T., Zhang, D., Zhou, Q., Ma, H.-X., Zhang, C., Hu, S., Li, Q.-L., Lin, Y., Li, X.-H., Wu, F.-Y., 2022. Geochemistry of impact glasses in the chang'e-5 regolith: constraints on impact melting and the petrogenesis of local basalt. Geochim. Cosmochim. Acta 335, 183–196.
Yang, J., Ju, D., Pang, R., Li, R., Liu, J., Du, W., 2023. Significance of silicate liquid immiscibility for the origin of young highly evolved lithic clasts in Chang'E-5 regolith. Geochim. Cosmochim. Acta 340, 189–205.
Yao, Y., Xiao, C., Wang, P., Li, C., Zhou, Q., 2022. Instrumental neutron activation analysis of Chang'E-5 lunar regolith samples. J. Am. Chem. Soc. 144, 5478–5484.
Zeng, X., Li, X., Liu, J., 2022. Exotic clasts in chang'e-5 regolith indicative of unexplored terrane on the moon. Nat. Astron. 7, 152159.
Zhang, D., Su, B., Chen, Y., Yang, W., Mao, Q., Jia, L.-H., 2022. Titanium in olivine reveals low-Ti origin of the Chang'E-5 lunar basalts. Lithos 414–415, 106639.
Zhang, J., Yang, W., Hu, S., Lin, Y., Fang, G., Li, C., Peng, W., Zhu, S., He, Z., Zhou, B., Lin, H., Yang, J., Liu, E., Xu, Y., Wang, J., Yao, Z., Zou, Y., Yan, J., Ouyang, Z., 2015. Volcanic history of the imbrium basin: a close-up view from the lunar rover Yutu. Proc. Nat. Acad. Sci. 112, 5342–5347.
Zhao, S., Xiao, L., Qian, Y., Zhao, J., She, Z., He, Q., Wang, Z., Wang, X., Cao, K., Zeng, X., Wang, Y., Sun, J., Dong, M., Xiao, Q., Yin, Z., Yang, H., Zhao, J., Wang, J., Huang, J., Hu, Z., Zong, K., Wu, X., Wang, C., 2023. Variations in lunar regolith properties with depth as revealed by chang'e-5 samples. Icarus 406, 115766.
Ziethe, R., Seiferlin, K., Hiesinger, H., 2009. Duration and extent of lunar volcanism: comparison of 3D convection models to mare basalt ages. Plan. Space Sci. 57, 784–796.
Zong, K., Wang, Z., Li, J., He, Q., Li, Y., Becker, H., Zhang, W., Hu, Z., He, T., Cao, K., She, Z., Wu, X., Xiao, L., Liu, Y., 2022. Bulk compositions of the Chang'E-5 lunar soil: insights into chemical homogeneity, exotic addition, and origin of landing site basalts. Geochim. Cosmochim. Acta 335, 284–296.